

Warmer and Wetter Winters over the high-latitude North Atlantic

an atmospheric circulation perspective



Siiri Wickström

Thesis for the degree of Philosophiae Doctor (PhD)
University of Bergen, Norway
2020

UNIVERSITY OF BERGEN



Warmer and Wetter Winters over the high-latitude North Atlantic

an atmospheric circulation perspective

Siiri Wickström



Thesis for the degree of Philosophiae Doctor (PhD)
at the University of Bergen

Date of defense: 19.05.2020

© Copyright Siiri Wickström

The material in this publication is covered by the provisions of the Copyright Act.

Year: 2020

Title: Warmer and Wetter Winters over the high-latitude North Atlantic

Name: Siiri Wickström

Print: Skipnes Kommunikasjon / University of Bergen

**Warmer and wetter winters over the
high-latitude North Atlantic**

-

**an atmospheric circulation
perspective**



Figure 0 'Lavtrykk i Arktis' by Erik M. Næss

Scientific environment

This study was carried out at and funded by the University Centre in Svalbard (UNIS). During this work I've been enrolled as a doctoral student at the Geophysical Institute, University of Bergen (UiB). Additional support was provided by the Norwegian Research Council Project 280573 'Advanced models and weather prediction in the Arctic: enhanced capacity from observations and polar process representations' (ALERTNESS) for my research visit to University of Colorado, USA. The Academy of Finland (contract 317999) funded one of my visits to the Finnish Meteorological Institute (FMI), Finland. During my doctoral training I have been enrolled in the research school on 'Changing climates in the coupled earth System' (CHESS) through which I had the chance to take several relevant courses. My supervisors are Marius O. Jonassen (UNIS, UiB) and Timo Vihma (FMI, UNIS).



FMI



Alertness



Acknowledgements

This thesis is a result of teamwork and would not have been possible without the great support that I have received over the past years from colleagues, friends and family. First of all, I want to thank my main supervisor, Marius O. Jonassen, for continuous encouragement, invaluable guidance and patience. It has been great fun to work with you, and I am truly grateful for this opportunity I have had to pursue my interests and learn from and with you along the way. I also want to thank Timo Vihma, my co-supervisor, for supervising my work with an endless enthusiasm and for bringing in your experience and wise guidance when Marius and I have been in doubt. Marius and Timo, it has been a great pleasure and an honor to have you as my supervisors. I also want to say thank you to my co-authors John Cassano and Petteri Uotila; this thesis would not have been possible without your help and support. My research exchange to John's lab at the University of Colorado in Boulder was one of the most special highlights both personally and professionally during this project; thank you, John!

UNIS has always felt like home and will always have a special place in my heart. I want to thank everyone at UNIS for making this such a warm and friendly working place that one always wants to return to. I especially want to thank the department of Arctic Geophysics that feels like a family to me. I'm grateful for having had the chance to be a part of this including, inspiring and supportive group of talented individuals. I want to thank everyone who has worked with me in the field and all the students in AGF-213 and AGF-350/850 over these years for a good time and valuable lessons. A special thanks goes to our technician Marcos for an enormous amount of help with the instrumentation (you are a true MacGyver!), and to my beloved ACSI-family: Ylva and Eli Anne.

Svalbard and UNIS can sometimes feel like a limited community when it comes to science, and I am deeply grateful for all the fantastic colleagues and friends I've met and worked with during my visits to FMI and CU. Also, a big thank you goes to the CHESSE research school for giving me a professional network outside Svalbard and introducing me to so many great PhD student peers during my doctoral training.

For the past four years Svalbard has been my home, and I am beyond words thankful for all my friends here on this spectacular island in the north. Thank you for being there for me in both good and bad times, thank you for all the love and laugh - you are all amazing and I love you so much. I especially want to thank Holt for helping me edit this thesis and for the countless ski trips. Thank you, Erik, for kindly making the beautiful front page illustration of Svalbard weather (Figure 0) - you are a true talent! Another huge thank you goes to Lilli and Erlend for feeding me and continuously cheering me up in the stressful final weeks of this work. I also wish to send lots of love to the Tuesday 08:30 am swimming club and to my friends back home - Minna, Vilma, Alex and Eero, thank you for always making me laugh and providing me with perspective in the ups and downs of life.

Last, but not least, I want to thank my family from all of my heart for always being there for me and supporting me unconditionally in my adventures. If you would not have taught me to work hard and dream big, I wouldn't be here today.

This would not have been possible without you all, thank you!

Introduction

The arctic climate system is a web of fascinating and complex air-sea-ice interactions where water in its frozen form can be found year-round in the Greenland Ice Sheet, glaciers, multi-year sea ice, and perennial snow. The dominance of ice in the Arctic is largely attributed to strong net surface heat losses during the polar night, when the sun remains below horizon for several months. Sea ice in particular plays a crucial role in the arctic climate system, as it isolates the atmosphere from oceanic heat and moisture, and reflects solar radiation much more strongly than the open ocean.

In this thesis I focus my attention on the atmospheric component of the intense air-sea-ice energy exchanges occurring over the high-latitude North Atlantic, especially in winter. Of primary interest for this work is the area surrounding the Svalbard archipelago located between Fram Strait, a part of the Greenland Sea, and Barents Sea. This region, situated at the nexus of both atmospheric and oceanic poleward heat transport pathways, has experienced warming in winter at some of the fastest rates observed globally. This winter warming has been accompanied by extensive winter season sea ice loss east and north of Svalbard, with critical implications for the arctic climate system.

Extratropical cyclones, commonly referred to as low pressure systems, traveling along the North Atlantic cyclone track are the main atmospheric heat source to the Arctic in winter. Warm, moist air transported polewards in these cyclones dramatically alters the thermal stability of the atmospheric boundary layer by cutting off lower atmospheric cooling and raising surface and lower-tropospheric temperatures. In extreme cases with warm enough air, cyclonic activity can result in rain-on-snow events and the onset of melt even in midwinter. The strength and orientation of the cyclone tracks, on which these low-pressures travel, thus exert a strong control on the regional climate. To address existing knowledge gaps and attempt to better understand the role of atmospheric circulation on the arctic climate system as a whole, this thesis is broadly

motivated by the need to find out how atmospheric circulation around Svalbard has changed over the last decades. This work further examines if - and if so, by which mechanisms - circulation changes are connected to the observed extreme winter warming rates and sea ice loss.

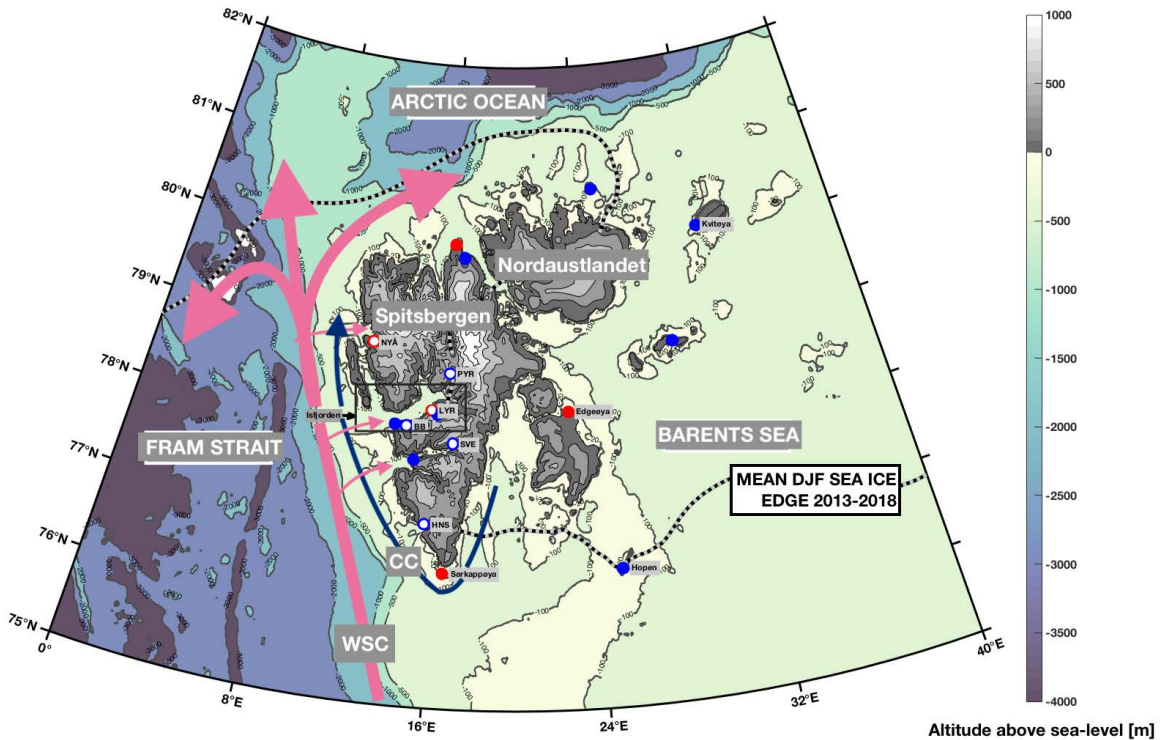


Figure 1 Map of Svalbard. The dots (red and blue) represent locations of permanent mast-based weather stations. The stations marked by red dots are used in this thesis for model validation and local variability studies. The dots with a white filling represent settlements, with year-round human activity (NYÅ = Ny-Ålesund, PYR=Pyramiden, LYR =Longyearbyen, BB = Barentsburg, SVE =Svea and HNS = the Polish research station in Hornsund). The light red arrows mark the West Spitsbergen Current (WSC) transporting warm and saline water masses northwards and the dark blue arrow mark the cold and fresh coastal current (CC). The location of these currents is reproduced according to Carmack et al. (2015) and Muckenhuber et al. (2014) and should be viewed as schematics and not an exact position of these currents. The 2013-2018 DJF mean sea ice extent (gray-black-line) is based on data from the Operational Sea Surface Temperature and Sea Ice Analysis -system (OSTIA)(Donlon et al. 2012).

Abstract

The high-latitude North Atlantic -especially the Svalbard archipelago and its surrounding seas - has undergone remarkable changes in the last half-century. These regions are recognized as a hotspot of the Arctic Amplification (AA), referring to the faster warming rates in the Arctic when compared to lower latitudes, manifested in the form of rapid warming and sea ice loss. The most pronounced changes occur in winter, when the sun remains below the horizon, and heat transport from lower latitudes in both atmosphere and ocean is the main energy source. The relationship between atmospheric circulation changes and the AA is not fully understood, and there are knowledge-gaps in particular on the regional scale. This thesis is motivated by the wish to quantify cyclone track changes and increase the knowledge of their role in the documented rapid temperature increases in Svalbard and the sea ice losses in north and east of this archipelago.

We utilized an automated cyclone tracking algorithm to create a seasonal cyclone climatology for the high-latitude North Atlantic in the period 1979-2016 based on the mean sea-level pressure from the reanalysis product ERA-Interim from the European Centre of Medium-Range Weather Forecasts (ECMWF). When calculating the trends over this period we find an increase of cyclone densities around Svalbard and a corresponding decrease in the southeastern Barents Sea of a magnitude ± 3 cyclones/winter per decade. Based on composite analysis, we find that these changes are in line with a trend towards warmer and wetter winter conditions in the northern Barents Sea and over Svalbard. The opposing trends, i.e. no significant changes in cyclogenesis and an increase in local baroclinicity north of Svalbard, all speak for a shift towards a more meridional winter cyclone track in the seas around Svalbard.

To advance the understanding of local 2-m air temperature and precipitation sensitivity to atmospheric circulation in the recent climate, with more winter cyclones around Svalbard, we studied the period 2013-2018 with a high-resolution numerical weather prediction model. The main finding of this study, forming a part this thesis, is that in the current climate, potentially high societal impact, rain-on-snow (ROS) events are

common phenomenon in the recent Svalbard winters with up to 11 events per winter in the southwestern parts of the archipelago. The clear majority of events with widespread ROS (in this study defined as more than 3% of Svalbard's land grid points experiencing ROS) occur with southerly and southwesterly flow over Svalbard. These flow directions occur in situations with a cyclone in southern Fram Strait - a region with a positive cyclone trend in the 1979-2016 winter climatology.

On a regional scale the warming has been largest in the northern and eastern parts of the Svalbard archipelago. We report extreme winter warming rates up to 3 K/decade in the north accompanied by significant ($p < 0.05$) increases in both accumulated precipitation (+ 44.6 mm/decade) and the number of precipitation days (+5.2 days/decade) over the period 1960-2017 based on the Norwegian hindcast product NORA10. The warming is significant, but only half of that in magnitude in the southern and western parts of the archipelago. We found the local warming and wettening in the north to correlate well with sea ice changes north of the archipelago and this is attributed to upwind changes of northeasterly flow. This effect is, however, further enhanced by a moderate, but significant increase in northerly winds aligning with the increased frequency of winter season meridional flow.

List of Publications

PAPER I

Wickström, S., Jonassen, M. O., Vihma, T., & Uotila, P. (2019): "Trends in cyclones in the high-latitude North-Atlantic during 1979-2016", *Quarterly Journal of the Royal Meteorological Society* 1–18. <https://doi.org/10.1002/qj.3707>

PAPER II

Wickström, S., Jonassen, M. O., Cassano, J. J., & Vihma, T. (2019): "Present temperature, precipitation and rain-on-snow climate in Svalbard", In review in *JGR: Atmospheres*

PAPER III

Wickström, S., Cassano, J. J., Jonassen, M. O., & Vihma, T. (2020): "Air temperature and precipitation trends in Svalbard affected by sea ice decline and changes in atmospheric circulation. In review to *JGR: Atmospheres*

Reprints were made with permission from Wiley and the American Geophysical Union (AGU).

Contents

Scientific environment	3
Acknowledgements	4
Contents	12
Aim of the Study	13
Background	14
Extra-Tropical Cyclones & Atmospheric Circulation	14
The Changing Arctic Climate System	19
Data, Strategy and Methods	23
Cyclone Tracking	23
Atmospheric Circulation Calendar	25
Reanalysis Products	26
AROME-Arctic	27
Automatic Weather Station Observations	28
The Study Area	29
Local and Regional Impacts of Atmospheric Circulation Changes over the High-Latitude North-Atlantic	33
The North Atlantic Cyclone Track	33
Arctic Cyclones	34
Climatology and Trends	34
Local Impacts	36
Summary	38
Future perspectives	44

Aim of the Study

The overarching motivation of this study is *a) to quantify changes in synoptic-scale atmospheric circulation in the high-latitude North-Atlantic (Papers I and III), and b) to better understand how the regional climate in and around the Svalbard archipelago is affected by these changes (Papers I-III)*. These regions have experienced rapid warming and sea ice loss over the last decades, especially in winter, and have been identified as hotspots of the ongoing climate change. Located at the periphery of the North Atlantic cyclone track, the atmosphere over the high-latitude North Atlantic is strongly affected by extratropical cyclones bringing warm and moist air masses poleward. As a result of this climatological situation, understanding the role played by atmospheric circulation and cyclone activity in the alarming winter warming and moistening is crucial. The main goal of this thesis is thus to increase knowledge of the atmospheric circulation aspect of the arctic climate change on a regional scale around Svalbard.

Special attention is given to rapidly changing winter season temperatures and precipitation. The influence of synoptic-scale atmospheric circulation on potentially high-impact rain-on-snow events is highlighted in Paper II. As these relatively short-lived events can have season-long consequences for ecosystems, cryospheric processes and infrastructure, they demonstrate the considerable influence an individual cyclone event can have on Svalbard's environment. Paper I quantifies trends in atmospheric circulation and addresses the physical drivers behind these changes including various climate indices and baroclinicity. Paper III investigates the relative contributions of specific atmospheric circulation changes and shifting upwind conditions of frequent flow directions on patterns of winter warming and precipitation increases across Svalbard.

Background

This chapter introduces the reader to the scientific foundation of this work and provides the background knowledge necessary to understand the achievements of this thesis.

Extra-Tropical Cyclones & Atmospheric Circulation

Extra-tropical cyclones are responsible for the majority of weather - winds, precipitation and rapid temperature changes - in mid-and high-latitude regions. In everyday language these weather features are often referred to as low pressure systems, cyclones, or sometimes even just storms. In meteorological terms, however, storm is a measure of wind speed and is not a suitable synonym to a low pressure.

Cyclones play an important role in poleward transport of heat, moisture and momentum in the atmosphere. These ‘waves of weather’ are particularly important to the weather of regions such as western Europe, Scandinavia, and North America that are situated at the eastern margins of the large ocean basins, located downstream of the cyclone tracks running west-to-east over both the North Atlantic and the Pacific.

The study of extra-tropical cyclones, their dynamics, and their impact on both weather and climate dates back to the nineteenth and early twentieth centuries. In 1919, the Norwegian physicist Jacob Bjerknes laid the basis for our current understanding of the structure and life cycle of extratropical cyclones (Figure 2) (Bjerknes and Solberg 1922; Bjerknes 1919). Even today the surface-level air mass interfaces associated with cyclone activity are called fronts, a naming convention inspired by warfare in the aftermath of World War I. The classical Norwegian polar front theory outlined by Bjerknes is predicated on the presence of strong temperature gradients at these surface fronts, where wavelike disturbances form along the interface between cold polar and warmer mid-latitude air. The wind blows cyclonically around these disturbances (anti-clockwise in the northern hemisphere) parallel to the isobars - lines of constant atmospheric pressures. The cyclone itself moves eastward following upper-level westerly winds.

The leading edge of the wave, where warm air penetrates poleward, is referred to as the warm front and the rear edge of the wave where cold air moves southward is called the cold front. When the cold air undercuts the warmer, lighter air (the cold front “catches up” to the warm front), the resulting air mass boundary is called an occluded front and is related to cyclone decay (Bjerknes and Solberg 1922 ;Lynch et al. 2006).

To get an understanding of the synoptic scale, spatially extra-tropical cyclones cover typically an area with a diameter of 1000 km, whereas the frontal zones have a cross-section of hundreds of kilometers. The cyclone advances at a speed of 15-20 m/s, depending on the strength of the upper level winds (Figure 2). Temporally extratropical cyclones have a characteristic lifetime of 3-5 days (Dacre et al. 2012).

Although advances in dynamical meteorology have extended and modified the specifics, Bjerknes’ polar front theory still stands, in 2020, as a cornerstone of synoptic meteorology and forms a conceptual basis for our understanding of extra-tropical cyclones (Reed 1990).

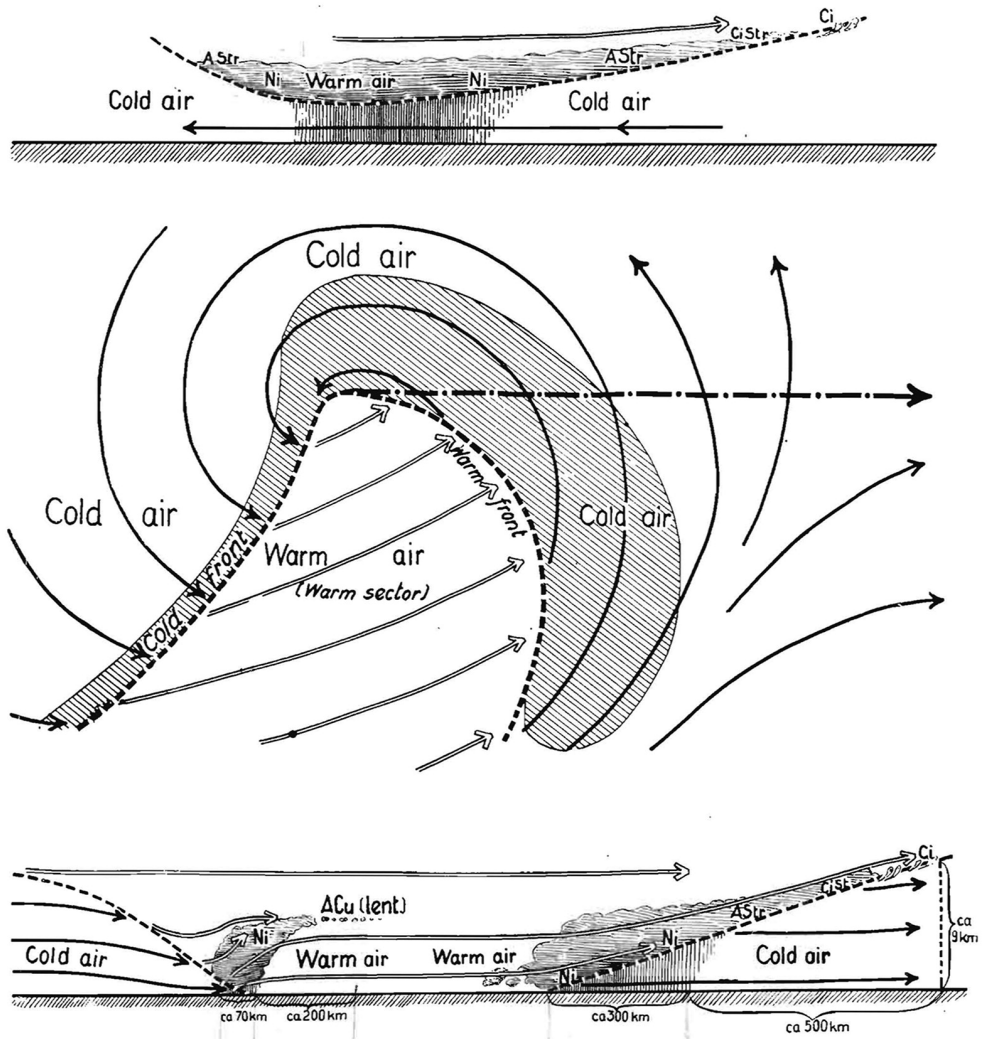


Figure 2 Idealized cyclone presented by the Bergen school (Bjerknes and Solberg 1922, their Fig. 1). The figure is provided through the courtesy of the Norwegian Geophysical Society.

Just before World War II, Carl G. Rossby laid the mathematical basis for describing the vertical structure of extra-tropical cyclones (Rossby 1939). Rossby showed that surface cyclone activity is connected to upper-level planetary waves, also known as

Rossby waves. These waves owe their existence to the north-south oriented planetary vorticity gradient and topography on our rotating Earth. Rossby's findings are an important part of the foundation of the modern understanding of atmospheric and ocean dynamic (e.g Gill 2016; Holton 1973). Rossby's mathematical work shows that the poleward advection of potential vorticity on the leading edge of a upper level trough helps facilitate surface cyclogenesis (birth of extra-tropical cyclones).

Following Rossby, pioneering work by Charney (1947) and Eady (1949) lead to the discovery of baroclinic instability -a sharp horizontal temperature gradient and/or strong vertical wind shear. Baroclinicity has a fundamental role in cyclogenesis and cyclone intensification. This theory helps explain why cyclones tend to form and intensify in regions with strong surface temperature gradients, and why their tracks, intensity and speed are determined by the upper-level jet stream (Shaw et al. 2016).

The eddy-driven jet stream, also known as the polar jet, provides the vertical wind shear component required to maintain baroclinic instability and nurtures mid-latitude cyclogenesis and cyclone intensification. This band of strong westerly winds is a product of eddy momentum flux convergence due to baroclinic waves, or, in other words, cyclone activity (Hoskins et al. 1983; Panetta and Held 1988). In addition to the polar jet, a thermally driven subtropical jet is found at the northern flank of the Hadley cell (Held and Hou 1980). Despite their different formation mechanisms, the polar and the subtropical jets are not always easy to tell apart. When the zone of the strongest baroclinicity occurs near the latitude of the subtropical jet, the two can merge; if the subtropical jet is weak and forms at lower latitudes, the two jets can be well-separated. The latter scenario is typically the case during the boreal winter over the North Atlantic when the storm track is at its strongest (Lee and Kim 2003). Additionally, in situations with the polar jet being found far south an Arctic Front jet may emerge at higher latitudes (Serebreny et al. 1962).

On a conceptual level, jet streams are physical manifestations of the thermal wind law, which states that a meridional temperature gradient produces vertical wind shear

normal to the gradient, when geostrophic balance in the horizontal and hydrostatic balance in the vertical applies. This theory explains why the westerly wind maxima at the jetstream core is found in the upper troposphere (12-15 km at the equator, 8-10 km in the polar regions) and why cyclones propagate eastward as they develop (Lynch et al. 2006; Holton 1973). The waves in this flow bring us back to Rossby and the planetary waves counteracting the meridional planetary vorticity gradient, linking surface weather to the vertical structure of the atmospheric column.

The Changing Arctic Climate System

This thesis is staged by dramatic pan-Arctic environmental changes that have occurred over the last half a century. The Arctic regions have undergone rapid climatic changes in the past decades, with atmospheric warming rates 2-4 times higher than what is observed globally (NOAA 2019;Cohen et al. 2014). This amplified warming is commonly referred to as ‘Arctic Amplification’ (AA) and is a key feature in both observed and modelled climate changes (Serreze et al. 2008; Screen and Simmonds 2010a; Cohen et al. 2014; Dai et al. 2019). This phenomenon is strongest in the winter season (Figure 3) and in the lowermost troposphere (Screen et al. 2013; Serreze et al. 2008). AA is furthermore clearly stronger than its southern hemispheric counterpart, the Antarctic warming (Turner et al. 2007; Marshall et al. 2014).

A number of phenomena and feedback mechanisms have been identified to contribute to AA. One of the most notorious drivers of AA are the feedback mechanisms and atmospheric interactions associated with diminishing Arctic sea ice cover (Figure 4) (Dai et al. 2019; Stroeve and Notz 2018; Screen and Simmonds 2010b; Vihma 2014; Onarheim et al. 2018). In addition to the central role of sea ice in the Arctic climate system and the well-known ice-albedo feedback mechanism (Thackeray and Hall 2019; Kashiwase et al. 2017), increased poleward heat transport both in the atmosphere (Cai 2005; Gong et al. 2017; Screen et al. 2018b; Zhang et al. 2008; Graversen et al. 2008) and the ocean (Chylek et al. 2009; Árthun et al. 2012; Spielhagen et al. 2011), dampened long-wave (LW) surface cooling due to the stability of the Arctic atmospheric boundary layer (ABL) (Bintanja et al. 2011; Pithan and Mauritsen 2014) and amplified LW surface warming due to increased atmospheric moisture and cloudiness (Park et al. 2015; Zhang et al. 2013; Naakka et al. 2019; Vihma et al. 2016; Nygård et al. 2019; Rinke et al. 2019) have been proposed, among other processes (Screen and Francis 2016; Ding et al. 2014), to contribute to AA. However, even though AA is captured and documented in a vast number of observational and model-based studies, the exact physical processes and their relative contributions remain a subject of debate (Dai et al. 2019; Kim et al. 2019). The central

components of the debate stem from questions associated with why AA is strongest in winter when darkness prevails and the ice albedo feedback is non-existent.

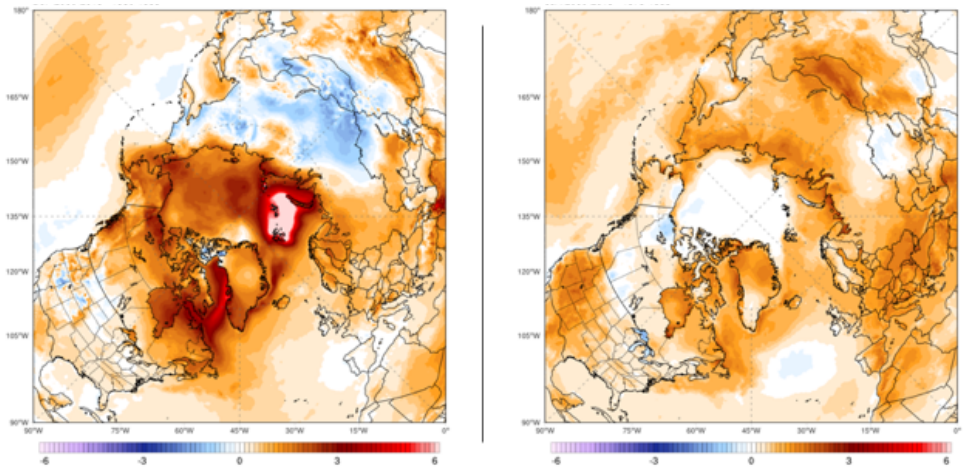


Figure 3) Difference between the mean a) winter and b) summer 2-m air temperatures [$^{\circ}\text{C}$] in the periods 1979-1999 and 2000-2019 (the anomaly is the latter period minus the former period; positive anomaly means warming in time). The data is from the Reanalysis product ERA5, the successor of ERA-Interim used in Paper I, from the European Centre of Medium-Range Weather Forecasts. Both images are reprinted with the permission of Climate Reanalyzer (<https://ClimateReanalyzer.org>), Climate Change Institute, University of Maine, USA.

What is known is that AA and the observed changes result from a number of complex interactions involving the atmosphere, ocean, land surfaces and the cryosphere. The complexity of the underlying processes makes filling existing knowledge gaps challenging. Challenges result from, among other things, a sparse observational network containing short and fragmented time series and a large internal interannual and decadal variability leading to large biases in modelled climate data. Although the Arctic is remote, limited in area, and sparsely populated, the arctic climate system's importance to the global energy balance combined with an increasing body of evidence showing linkages between AA and mid-latitude climate and weather (Deser

et al. 2017; Vihma 2014; Francis et al. 2017; Cohen et al. 2014; Tang et al. 2013; Cohen et al. 2019) demonstrate the global implications of rapid environmental changes in the high latitudes and make confronting these challenges necessary.

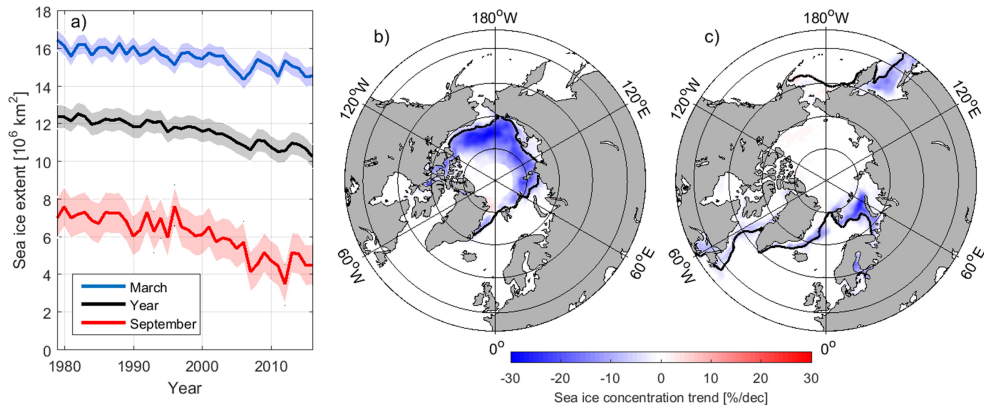


Figure 4) (a) March (blue), September (red), and annual mean (black) Northern Hemisphere sea ice extent, 1979–2016. Shaded regions indicate plus and minus one standard deviation. Linear sea ice concentration trends ($\% \text{ decade}^{-1}$) in (b) September and (c) March, 1979–2016. Black contours show the mean sea ice edge. This Figure is reprinted from (Onarheim et al. 2018) with the permission of American Meteorological Society (AMS).

Atmospheric circulation is a key element in the environmental linkages between the Arctic and the mid-latitudes (Barnes and Screen 2015; Walsh 2014). However, atmospheric circulation responses to the ongoing climate change are not well-established, especially at the regional scale (Screen et al. 2018b; Collins et al. 2018; Shepherd 2014). This is particularly true at high-latitudes where atmospheric variability associated with the annular modes of circulation remains poorly resolved and a considerable source of uncertainty (Deser et al. 2012).

On an Arctic-wide scale it is known that the Arctic Oscillation (AO), also known as the Northern Annular Mode (NAM), is the dominant mode of atmospheric variability (Thompson and Wallace 2000). A positive (negative) AO corresponds to strengthened (weakened) zonally averaged westerly winds due to anomalously low (high) surface

pressure over the Arctic and anomalously high (low) pressure over the mid-latitudes (Figure 5). Considerable progress has been made in the last decade with regards to understanding the impact Arctic sea ice has on the AO variability. Several studies have reported a positive correlation between Arctic sea ice and AO (Nakamura et al. 2015; Yang et al. 2016) and modelling studies support a causal link between these two (Deser et al. 2015; Smith et al. 2017; McCusker et al. 2017). Two mechanisms by which sea ice can force the AO are identified; one tropospheric and one stratospheric (Sun et al. 2015). The suggested stratospheric mechanism is linking low early winter ice-cover on Barents and Kara Seas and enhanced upward propagation of planetary waves leading to a weaker midwinter stratospheric polar vortex. A weak stratospheric vortex is found to preferentially induce negative AO (Nakamura et al. 2016; Kim et al. 2014). The tropospheric mechanism involves changing cyclone activity and cyclone track characteristics as a response to the changing meridional temperature gradient and baroclinicity (Wu and Smith 2016).

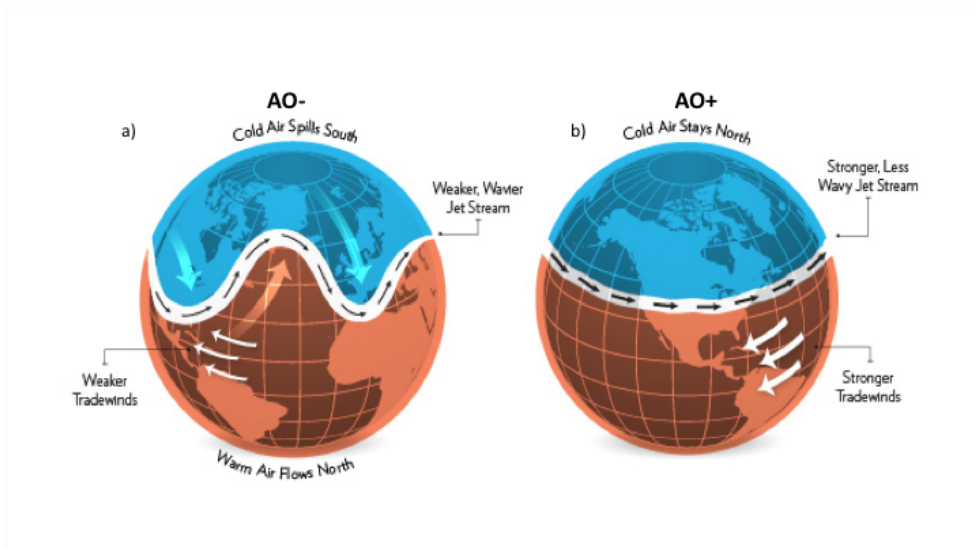


Figure 5) Conceptual model of a) negative and b) positive phases of Arctic Oscillation (AO). This simplified illustration does not separate the thermodynamically and eddy driven jet streams, but rather shows their joint contribution. This figure has been reprinted and modified with the permission from Weather Underground (<https://www.wunderground.com/>).

Data and Methods

This thesis employs model data both from reanalysis products (ERA-Interim from the European Centre of Medium-Range Weather Forecasts in Paper I and the Norwegian hindcast dataset NORA10 in Paper III) and the operational numerical weather prediction (NWP) AROME-Arctic (Paper II). Additional continuous weather data from automatic weather stations connect this work to actual observations.

Cyclone Tracking

Cyclone tracking refers to algorithm-based detection and tracking of extra-tropical cyclones, which produces information about both cyclone movement and qualities - including center pressure, radius and intensity - over time.

Automated cyclone tracking algorithms have gained popularity in global and regional scale cyclone activity studies since the early 1990's. On a conceptual level, cyclone tracking in the extratropics presents itself as a straightforward task. Unfortunately, this is not reality. The large variability in size, vertical structure, and intensity, combined with the rather complex dynamics of cyclone development, movement, and decay makes identifying and following these common features objectively a challenge (Neu et al. 2013). Situations where cyclones split or merge, thereby changing the number of tracked features, place particularly challenging demands on the tracking scheme and can induce error.

Today, a relatively large body of cyclone tracking schemes exists. These schemes vary in their methodologies by which they track and identify cyclones, reflecting the lack of a single commonly agreed scientific definition of an extratropical cyclone (Neu et al. 2013 and references within). Depending on how a cyclone is defined, a variety of atmospheric variables are used for tracking (Hoskins and Hodges 2002; Raible et al. 2010; Ulbrich et al. 2009). However, the vast majority of these algorithms use either mean sea-level pressure (MSLP) or low-tropospheric vorticity as the tracking metric (e.g. Sinclair 1994; Hodges et al. 2003; Rudeva and Gulev 2007; Ulbrich et al. 2009).

MSLP- and vorticity-based cyclone tracking algorithms approach cyclone activity differently: vorticity contains more information on the wind field and on the high-frequency synoptic scale, whereas MSLP is a measure of the mass field and a better representation of the low-frequency synoptic scale (Hodges et al. 2003). The tracks produced with these two variables are not expected to be identical. The vorticity-based center and the lowest surface pressure (MSLP center) do not always co-locate, nor are all mobile vorticity centers associated with a MSLP minimum (Sinclair 1994).

The cyclone tracking algorithm ran for Paper I in this thesis is based on MSLP fields (Murray and Simmonds 1991). An MSLP-based tracking algorithm is appropriate for addressing a research question tied to regional impacts of cyclone activity, as the MSLP field and near-surface conditions, including 2-m air temperatures, winds, and precipitation are closely tied together. The exact scheme used, the Melbourne University cyclone tracking scheme (Murray and Simmonds 1991), is one of the pioneering schemes shown to perform well in a number of comparison studies (Neu et al. 2013; Simmonds and Rudeva 2014), and has been previously employed in numerous peer-reviewed publications (Rudeva and Simmonds 2015; Simmonds and Lim 2009). This scheme scans a given MSLP field and compares the Laplacian of the pressure field between adjacent grid points. The Laplacian of the pressure field is interpreted as a measure of the cyclone intensity (Petterssen 1957). A given intensity is required for the algorithm to recognize a low pressure system. In the set-up ran for Paper I the threshold was set to $0.2 \text{ hPa} \cdot (\text{° latitude})^{-2}$ over a radius of 2° . In Paper I, we focus only on strong cyclones that have an average value of the Laplacian above $0.7 \text{ hPa} \cdot (\text{° latitude})^{-2}$ with a well-defined (closed) center. When a pressure depression is identified, the low pressure center is determined through an iterative process determining the ellipsoid with the best fit to the MSLP field (Murray and Simmonds 1991). Based on the cyclone's previous movement and climatological cyclone tracks, the algorithm makes a first guess of the cyclone location in the following time step. Scanning for MSLP depressions and locating their centers is repeated at each

subsequent time step, such that the pressure depression is followed throughout its evolution from appearance to decay.

Atmospheric Circulation Calendar

Considering the limitations accompanying automated cyclone detection presented above, one could argue that a thorough manual reanalysis of cyclone trajectories based on weather maps utilizing all available data (e.g., Hewson et al. 2000) would result in the best tracks. Such a methodology is not feasible in reality over large areas, nor is there a single ‘truth’ about a cyclones track. Hence, any results derived from such a manual reanalysis would be biased by the analysts’ interpretation. Manual classifications of MSLP fields have been found useful on regional and local scales, however. Arguably the best recognized of such datasets is the Lamb classification made for synoptic situations over the British Isles (Lamb 1972). Typically of a daily temporal resolution, these datasets are commonly called atmospheric circulation calendars. Despite being somewhat subjective, such datasets provide an avenue to study the local manifestation - mainly wind direction - of the atmospheric circulation patterns. The large variability in cyclone radii and shape makes it close to impossible to derive this information solely from cyclone track data.

Papers II and III focus on the atmospheric circulation aspect of the arctic winter warming regionally in and around Svalbard. In both of these studies, we use the “Niedźwiedz Classification” of atmospheric circulation patterns over Svalbard (Niedźwiedz, 2013). This classification is an atmospheric circulation calendar with 21 different synoptic situations identified manually using daily MSLP charts. This calendar is constructed with methods very similar to other well-recognized manual atmospheric circulation catalogs including the aforementioned Lamb and the Grosswetterlage (Hess and Brezowsky, 1952, 1969, 1977). The pressure charts used in this classification are synoptic maps published in “Tägliche Wetterbericht” (1950–1975), “Europäischer Wetterbericht” (1976–2000), and after 2000 on the DWD Archives (http://www.wetter3.de/Archiv/archiv_dwd.html). The calendar builds on determining the geostrophic wind direction over Svalbard based on the synoptic MSLP charts. The synoptic situations are classified based on the main geostrophic wind

direction, which is assessed from MSLP fields. The classification is based on 8 cardinal and ordinal wind directions labelled with capital letters (N = northerly, NE = northeasterly, E = easterly, SE = southeasterly, S = southerly, SW = southwesterly, W = westerly and NW = northwesterly). Further, the directions are divided into cyclone (c) and anticyclone (a) driven atmospheric circulation patterns. In practice, this means that the proximity of a cyclone or an anticyclone to Svalbard dictates whether a pressure pattern is classified 'a' or 'c' (e.g SWc = southwesterly geostrophic wind over Svalbard driven by low pressure in the vicinity of Svalbard or, SWa = again, southwesterly geostrophic wind over Svalbard but the flow is driven by high pressure in the vicinity of Svalbard). In addition to the 16 directional atmospheric circulation types, the calendar has four non-directional atmospheric circulation types (Ca = high pressure centre over or very near Svalbard, Ka = high pressure ridge, Cc = low pressure centre over or very near Svalbard, Bc = cyclonic trough) and one unclassified type, X.

Reanalysis Products

Reanalysis products are reruns of forecast models and data assimilation systems with archived observations, creating global data sets describing the recent history of the atmospheric, oceanic and land-surface state. Reanalyses provide consistent and convenient 'maps without gaps' used widely in climate and atmospheric sciences.

ERA-Interim

To revisit cyclone tracking briefly: It is not solely the quality of the tracking algorithm that defines the merit of the output. The resolution and model physics of the tracked dataset is the key to good results. The ERA-interim (ERA-I) reanalysis produced by the European Centre of Medium-Range Weather Forecasts (ECMWF) (Dee et al. 2011) is proven to perform well in the Arctic (Dufour et al. 2016; Koyama et al. 2017; Naakka et al. 2018), and therefore this dataset was chosen for the cyclone tracking in Paper I.

This dataset covers the period 1979 to 2019 and is run globally with a native grid spacing of 0.75 x 0.75 degrees and 6-hourly temporal resolution.

NORA10

Paper III is built on the finer-scale regional reanalysis product NORA10. This product is a hindcast run from 1960 to present in a 11x11 km grid (Reistad et al. 2011; Breivik et al. 2013). NORA10 is based on the numerical weather prediction model High Resolution Limited Area Model (HIRLAM) version 6.4.2 (Undén et al. 2002). HIRLAM was forced with the global reanalysis ERA40 from ECMWF until 2002 (Uppala et al. 2005), and thereafter with data from the global NWP model ECMWF IFS.

AROME-Arctic

AROME-Arctic is a short-range high-resolution operational weather model for the European Arctic run and developed by the Norwegian Meteorological Office (MET Norway) (Køltzow et al. 2019; Müller et al. 2017). The model domain includes the northern part of Norway and surrounding islands, the Barents Sea, the Svalbard archipelago, and parts of the Greenland Sea. This model has a horizontal grid spacing of 2.5 km and 65 vertical levels, 20 of which are located below 1 km. The lowermost vertical level is found at only 11 m and the upper boundary (highest vertical level) is located at 9 hPa (24 km). AROME-Arctic is a non-hydrostatic model, meaning that the model solves the vertical momentum equation and is able to resolve mesoscale circulations, such as the sea breeze. At the basis of this model, lies the HARMONIE-AROME configuration of the ALADIN-HIRLAM numerical weather prediction system (Bengtsson et al. 2017).

AROME-Arctic has been run for research purposes since October 2012, and operational use started in June 2017. The model issues deterministic forecasts four times per day (00 06 12 18 UTC) with a 66 hour lead time. AROME-Arctic uses the hourly ECMWF HRES forecasts for forcing at its lateral boundaries, and also

assimilates ECMWF sea ice concentration and sea surface temperatures into the model (Batrak et al. 2018).

Automatic Weather Station Observations

Data from automatic weather stations (AWS) are used in this thesis to validate the performance of the regional-scale model data from AROME-Arctic and NORA10 on 2 m air temperature and precipitation. We chose stations from the network of available AWS in Svalbard that are representative of the cardinal wind directions (North, East, West and South) and one central station (shown in Figure 1).

The Study Area

This thesis focuses on regional scale changes in atmospheric circulation in the European Arctic, comprising the northernmost portion of the North Atlantic.

Investigating changes in the area surrounding the remote Svalbard archipelago forms the center of this work, as most of the observational time series in the European Arctic are from Svalbard.

Svalbard is located at a hotspot of converging atmospheric and oceanic poleward heat transport pathways making this region of great interest both for the global heat balance and air-sea-ice interactions. From an oceanic perspective, the West Spitsbergen Current (WSC) transports warm Atlantic Water masses northward just off Svalbard's west coast (Carmack et al. 2015; Aagaard and Greisman 1975), while in the Barents Sea east of Svalbard warm Atlantic water inflow in the Norwegian Atlantic Current is much farther from Svalbard. Large parts of the Barents Sea region near Svalbard thus bear a seasonal ice cover, unlike the perennially ice-free eastern Fram Strait (Carmack et al. 2015; Smedsrud et al. 2013) (Figure 1). In the atmosphere, the North Atlantic cyclone track approaches Svalbard from the southwest bringing mid-latitude air masses to the Arctic. Depending on the orientation of the polar jet during the winter months, the cyclones tend to follow one of two branches: either a meridional path northwards into and through the Fram Strait or a more zonal pathway eastward into the southern Barents Sea (Figure 7 a,c,g). This pattern disappears in the summer when the cyclone track is at its weakest (Figure 7 e). Both in the atmosphere and in the ocean the poleward heat transport is strongest in the Atlantic sector (Schlichtholz 2018).

Svalbard's topography is predominantly mountainous, with mountain ranges interspersed by glaciofluvial incised valleys and, along the coastlines, expansive fjord systems terminating in many locations in marine glaciers. The mountaintops lie primarily below 1000 m in most parts of the archipelago, with higher peaks found in the more mountainous glaciated northern and northeastern parts of the region (Figure 1).

The relatively pleasant climate in the vicinity of the warm WSC has concentrated human activity at or close to Svalbard's west coast. Half of the six permanently inhabited settlements - Longyearbyen, Barentsburg and Pyramiden - are located at the coasts of the side fjords of Isfjorden, Svalbard's largest fjord system. The remaining three settlements are also all found in fjord systems along the western coast: Ny-Ålesund in Kongsfjorden, a Polish research station in Hornsund and the mining settlement Svea in Van Mijenfjorden, where efforts are currently underway to depopulate and shutter the community (Figure 1). The spatial imbalance and concentration of anthropogenic presence near the western coast of Svalbard is reflected in a data-availability bias towards these locations. Thus, knowledge of Svalbard's climate, based on observations, is biased towards this relatively small portion of the archipelago, while the climatic conditions of the northern and eastern parts of the archipelago are less well known.

Surrounded by warm atmospheric and oceanic currents, Svalbard is the warmest and wettest location at latitudes between 76 N and 80 N (Serreze and Barry 2014). As a result of this high-latitude location, the sun in Svalbard remains below the horizon between late-October and mid-February during the polar night and, on the other end of the spectrum, does not set in the period between mid-April and mid-August. Mean temperatures in all seasons have a strong southwest-northeast oriented gradient with the lowest temperatures found in mountainous and heavily glaciated areas in the northeast (Figure 6). This temperature gradient is at its maximum in winter when the presence of sea ice lowers air temperatures to the east and the open ocean moderates' temperatures in western portions of the archipelago (Figure 6). The precipitation gradient is also zonal, with more precipitation falling at the west coast (Hanssen-Bauer et al. 2019).

The annual mean 2-m air temperature in Svalbard was -8.7 C during 1971-2000. Seasonally averaged air temperatures are below zero in all seasons except summer, when they average 0.5 C (1971-2000). No observational precipitation data exists for areas outside the settlements on the west coasts in official records. The modeled annual mean precipitation for the entire archipelago is 723 mm (1971-2000) with the

majority (225 mm) falling in the fall (1971-2000). Annual modeled precipitation increased 29 mm between the 1961-1990 and the 1971-2000 30 year normal periods, averaged across the archipelago. The increase is largest in the northwestern part of the archipelago with an 31 mm increase in annual modeled precipitation between the normal periods (Hanssen-Bauer et al. 2019).

Cyclonic flow dominates on an annual scale over Svalbard, largely due to Svalbard's close proximity to the North Atlantic cyclone track. Cyclonic flow is most dominant in the winter. The prevailing wind direction over the archipelago is from the eastern sector as a consequence Svalbard's location relative to the low pressure systems in the Norwegian Sea (Isaksen et al. 2016; Hanssen-Bauer et al. 2019).

2-m air temperatures measured at Longyearbyen airport increased by 4.0 °C during the period 1971-2017, compared to a 0.83 °C global increase (NOAA National Centers for Environmental Information, 2019). This warming is most pronounced in winter, as wintertime air temperatures increased by 7.8°C during 1971-2017, translating to a 1.7° C per decade winter warming trend (Hanssen-Bauer et al. 2019). Regional reanalyses indicate even higher warming rates in the northern and eastern parts of the archipelago, with some studies suggesting rates of 1.8°C per decade during 1971-2000 (Hanssen-Bauer et al. 2019). An increase in the number of winter rain events in addition to the total accumulated winter precipitation have accompanied this warming trend (Vikhamar-Schuler et al. 2016; Hansen et al. 2019; Hanssen-Bauer et al. 2019).

Sea ice conditions surrounding the archipelago have also changed dramatically over the last half-century. Notably, increased warm Atlantic Water inflow following changes in atmospheric circulation promoting more meridional flow in the Fram Strait (Nilsen et al. 2016; Cottier et al. 2007) has been hypothesized to have resulted in the fjords along the west coast remaining ice-free throughout the winter in recent years (Muckenhuber et al. 2016). Extensive winter sea ice losses are also reported in the Arctic Ocean and Barents Sea to the north and east of Svalbard, respectively (Onarheim et al. 2014, 2018; King et al. 2017) (Figure 4).

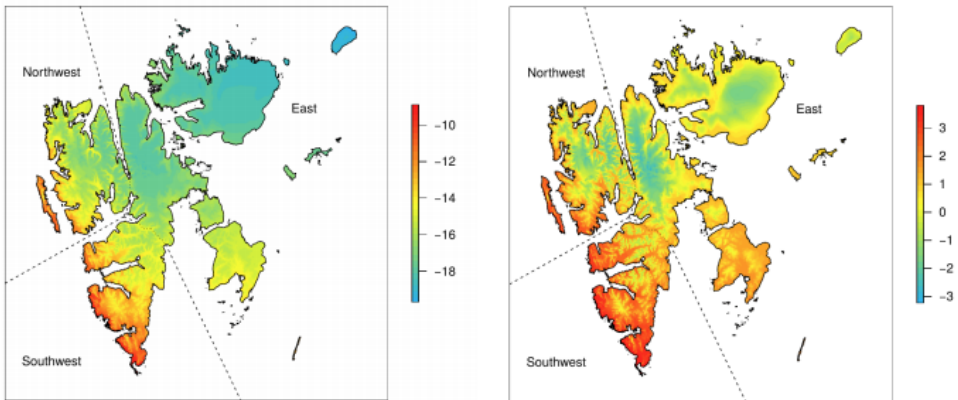


Figure 6) Svalbard mean 2-m air temperatures [$^{\circ}$ C] winter (DJF) in the left panel and summer (JJA) in the right panel during (1971-2000). Note: Colorbar scales are not the same. The figure is courtesy of Hanssen-Bauer et al. 2019.

Local and Regional Impacts of Atmospheric Circulation Changes over the High-Latitude North Atlantic

This chapter puts the results attained in this thesis into the context of the current knowledge on atmospheric circulation changes and their impacts, focusing on the North Atlantic sector of the Arctic.

The North Atlantic Cyclone Track

The vast majority of the winter season extra-tropical cyclones reaching Svalbard and the high-latitude North Atlantic originate from lower latitudes (Sepp and Jaagus 2011; Sorteberg and Walsh 2008; Zhang et al. 2004). Most of these cyclones are born over regions of enhanced baroclinicity off the eastern coast of the North American continent or around the southern tip of Greenland and Iceland (Hall et al. 2015). Strong baroclinic zones in this region are often a product of cold continental air masses flowing over a relatively warm ocean or sharp sea surface temperature (SST) gradients usually related to the Gulf Stream (Brayshaw et al. 2011; Minobe et al. 2010). The exact location of the storm track is also affected by orographic features, which in the North Atlantic framework consist primarily of the Rocky Mountains and Greenland (Vallis and Gerber 2008). These features deflect the prevailing westerly flow southwards, giving the North Atlantic cyclone track its southwest-northeast orientation as this meridional bend is propagated westwards (Brayshaw et al. 2009).

Understanding the North Atlantic cyclone track's response to the ongoing climate change is key to grasping circulation changes affecting the Svalbard region. As previously mentioned, arctic sea ice extent correlates positively with AO. In line with this, (Screen et al. 2018a) showed a consistent equatorward shift in cyclone tracks with decreasing sea ice in coupled climate model experiments. However, previous work from the same author (Screen et al. 2014) reported difficulties in detection of the southward storm track shift for the period 1979-2009 due to model-dependencies and masked inter-annual variability. However, sea ice extinction is not the full story when

it comes to greenhouse gas created climate change. Attributed to increased upper level tropical heating (Butler et al. 2010) and warmer sea surface temperatures (Graff and LaCasce 2014) among other mechanisms, an opposing poleward shift of the mid-latitude cyclone tracks has been reported as a response to anthropogenic greenhouse-gas forcing (Chang et al. 2012; Woollings et al. 2012; Tamarin and Kaspi 2017; Yin 2005). This shift is reported to be on the order of 1° to 2° latitudinal poleward shift in a CO₂ doubling scenario (Chang et al. 2012).

In the context of this thesis, the results in Paper I indicate a trend towards a more meridional winter cyclone track over the high-latitude North Atlantic in the period investigated (1979-2016), with more cyclones around Svalbard. This result supports qualitatively a transition towards a wavier jet, associated negative AO and southward cyclone track shift.

Arctic Cyclones

Climatology and Trends

The number of cyclones peaks on an Arctic-wide scale in the summer, with a maximum cyclone frequency in the central Arctic (Serreze and Barrett 2008). During this season, cyclones tend to intensify over the Eurasian continent where the sharp boundary between relatively warm continental and relatively cold maritime air masses acts as a baroclinic zone (Crawford and Serreze 2016). The transition towards colder seasons and the corresponding strengthening of the polar jet stream later in the year activates the North Atlantic cyclone track, and cyclone densities increase over the Greenland, Norwegian, and Barents Seas. In fall and winter, this cyclone track is the main source of cyclones reaching the Arctic (e.g., Zhang et al. 2004).

A growing number of studies have addressed the question of how cyclone activity has changed in the Arctic (Rudeva and Simmonds 2015; Zahn et al. 2018; Rinke et al. 2017; Sepp and Jaagus 2011; Zhang et al. 2008; Wei et al. 2017; Simmonds et al. 2008; Koyama et al. 2017). The findings of these studies qualitatively agree on a generalized pattern of an increase in winter cyclones north of both Greenland and the

Canadian Arctic Archipelago as well as around Svalbard, while decreased cyclone activity is found in the Barents Sea and north of the Russian coast (Zahn et al. 2018; Rudeva and Simmonds 2015). A recent study by Parding et al. (2019) found a similar winter bipolarity with a positive cyclone density trend around Svalbard and a negative trend in southern Barents Sea. Also Rinke et al. (2017) found, based on automatic weather station data, an increase in winter cyclone activity in Svalbard. These reported winter changes align well with recent work on high-latitude blocking events (Luo et al. 2019). The studies that included fall and spring trends report somewhat similar, but lower magnitude, trends compared to the winter trends (e.g Parding et al. 2019). In summer, cyclones are found to decrease in the central Arctic north of the Beaufort Sea and increase over the Laptev Sea (Zahn et al. 2018; Rudeva and Simmonds 2015). As trends in different regions of the Arctic are often of an opposing sign during the same season, no single season shows a significant net trend in cyclone activity when considering the Arctic as a whole (Wei et al. 2017; Simmonds et al. 2008).

In general, the reported changes are relatively small in magnitude and only a handful of the regional trends are significant ($p < 0.1$ widely used in these studies). This is first and foremost a manifestation of the turbulent nature and the associated high inter-annual variability of cyclone activity. Similarly, it has been shown that these results are somewhat sensitive to the choice of reanalysis product, tracking scheme, and the exact study period. Simmonds and Rudeva (2014) compared the results of ten tracking schemes in the Arctic and found agreement in cyclone center location, but deviations of up to 10 hPa in cyclone depths. Zahn et al. (2018) compared four different reanalyses and discovered the sign of the trends and their spatial distribution to match well, although the magnitudes of the trends in different regions strongly varied across the reanalyses. The contrasting trends regionally were consistent across the data.

With the exception of Koyama et al. (2017), none of these studies explicitly investigates the drivers behind these regional changes. Koyama et al. (2017) studied the connection between arctic sea ice and cyclone activity but found no robust results between the cyclone count and sea ice presence. However, increased potential for cyclone intensification and cyclogenesis through enhanced baroclinicity is reported in

regions where sea ice retreat allows free transfer of heat and moisture at the air-ocean interface.

Local Impacts

The local and regional impacts of cyclone activity in the Arctic are to a large degree a product of air-sea-ice interactions. As shown by Koyama et al. (2017), sea ice retreat enhances atmosphere-ocean heat and moisture exchange as well as local baroclinicity. Furthermore, cyclones bring in warmer air, clouds and precipitation - conditions which stall or even reverse sea ice growth. Precipitation has impacts on sea ice mass balance: if the precipitation falls as rain, it lowers the surface albedo, while if it falls as snow it isolates the ice from the cold atmosphere and reduces ice growth (Graham et al. 2019).

Individual cyclones are rather small and short-lived features on a global scale, however on a regional-to-local scale they can have extreme impacts with cascading effects in time and space. For example, the Great Arctic cyclone preconditioned sea ice conditions in such that the all-time record low sea ice extent was reached in 2012 (Simmonds and Rudeva 2012). Another example of a winter cyclone reaching the Arctic from the North Atlantic is the storm Frank in early 2016. Warm and moist air masses associated with this cyclone penetrated exceptionally far north, with temperatures at the North Pole reaching above freezing (Kim et al. 2017). These conditions led to an all-time winter sea ice minimum in 2016, driven by sea ice thinning and retreat due to cyclone activity (Boisvert et al. 2016). High winds and precipitation attributed to the same warm and moist intrusion as the storm Frank, also led to a fatal avalanche in Longyearbyen, Svalbard in December 2015 (Hancock et al. 2018).

A cyclone passage deteriorates sea ice through a variety of mechanisms. The thick frontal cloud associated with the warm sector of the low-pressure reverses the longwave radiative flux at the surface (Graham et al. 2017). Longwave cooling is one of the main mechanisms by which sea ice loses energy to space and a stably stratified atmospheric boundary-layer (ABL) is sustained. This stable stratification, often manifested as a surface based temperature inversion (Mäkiranta et al. 2011), shields

the snow and ice covered surfaces from warmer air above. This stable layer breaks down when subjected to thermal radiation from clouds and mixing by winds, and warmer air can thus reach the surface. In addition to wind-enhanced mixing, which drives turbulent surface fluxes, wind also mechanically breaks and physically transports sea ice. Wind is especially effective at breaking and transporting young and thin sea ice. Graham et al. (2019) showed that northerly winds at the western side of a cyclone north of Svalbard can enhance basal sea ice melt as it advects the ice over the warm West Spitsbergen Current in the south (Figure 1).

Aforementioned case studies of high-impact cyclones have spurred studies on extreme cyclones and their trends (Rinke et al. 2017; Koyama et al. 2017). Just as with extra-tropical cyclones, there are also multiple definitions as to what constitutes an extreme cyclone. Rinke et al. (2017) defined cyclones with a surface pressure below 985 hPa as extreme. Based on 6 hourly station data from Ny-Ålesund, Svalbard, their study reported an increase of 6 extreme winter cyclones/decade in the period 1979–2015. Koyama et al. (2017) used cyclone tracking data and defined extreme cyclones as cyclones with a center pressure 40 hPa lower than the climatological mean in each grid point (following Vavrus et al. 2013 and Chang et al. 2012). This study covered the period 1979-2014 and found a negative, but not significant, trend in winter extreme cyclones in the Greenland, Norwegian, and Barents Seas. Interestingly, Koyama et al. (2017) reports a significant positive correlation between low sea ice years and extreme cyclones in the Fram Strait, the region investigated by Rinke et al. (2017). Further, Koyama et al. (2017) reports a significant ($p < 0.001$) positive correlation of 0.52 between AO and extreme cyclones in the Greenland, Norwegian, and Barents Sea region, suggesting that positive AO-related increases in baroclinicity and cyclogenesis potentially promote an increase in extreme cyclones in the Arctic.

Summary

Atmospheric circulation strongly influences the regional climate in the Arctic, as demonstrated in this thesis. In the following synthesis, I summarize the main findings of this thesis and contextualize them within the current knowledge in the field.

Paper I presents to my knowledge the most up-to-date storm-track-based cyclone density climatology for the northern North Atlantic (Figure 7). This study is based on 6-hourly cyclone track data derived from ERAI MSLP fields from 1979-2016. The results align well with the existing body of literature, showing an increase in cyclone activity over Svalbard and a corresponding decrease in the southeastern Barents Sea over the last 30-40 years. As expected, based on previous work, even the strongest significant changes are modest in magnitude - with 3 more winter cyclones over Svalbard per decade. However, even modest changes can have substantial impacts, given the potential season-long consequences of individual cyclone events. The composite analyses linked storm track changes to local and regional weather and climate conditions. Our results demonstrate the local consequences of cyclone paths by showing how sharp horizontal gradients in precipitation, temperature, pressure and energy are controlled by the mean cyclone center location. Based on the composites, the reported trends show a tendency towards warmer and wetter conditions around and north of Svalbard. This is supported by a significant, but relatively modest increase in meridional cyclonic flow over Svalbard (Paper III). Paper I is also the first study to specifically investigate the drivers of the regional bipolarity in winter cyclone tracks found in the Barents Sea. Our results indicate that the regional shift towards a more meridional winter storm track is associated with a positive trend in the Scandinavian Pattern. This result is supported by Woods and Caballero (2016) who showed that warm and moist intrusions into the Arctic often occur on the upstream side of an atmospheric blocking pattern. Furthermore, we find a significant decrease in the Brunt-Väisälä frequency east of Svalbard and a significant increase in the Eady Growth Rate north of Svalbard indicate increased baroclinicity, favoring enhanced cyclone activity in these regions.

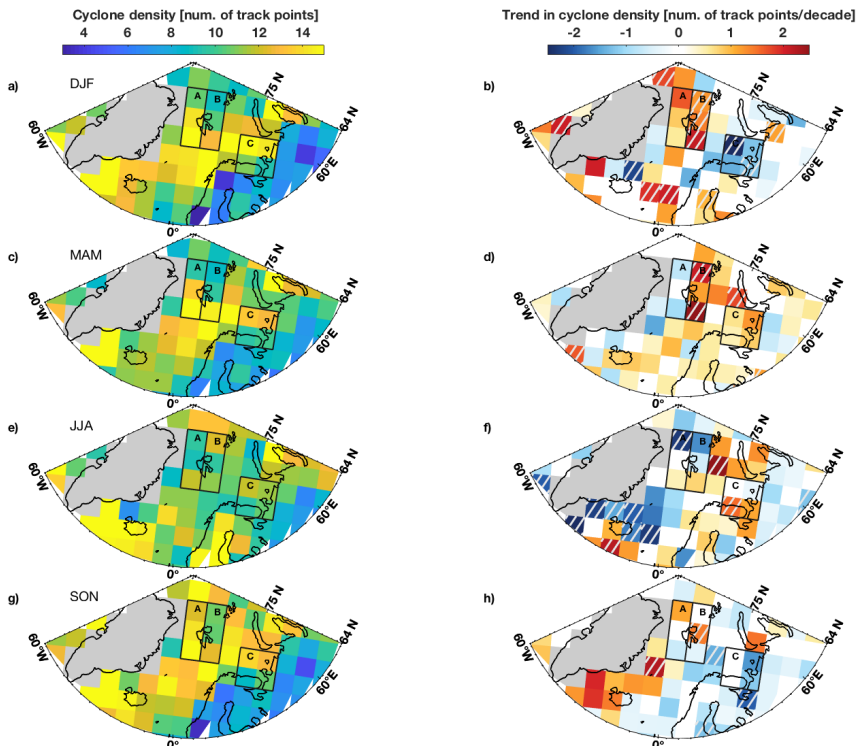


Figure 7) Mean cyclone density and the cyclone density trend in a-b) winter (DJF), c-d) spring (MAM), e-f) summer (JJA) and g-h) fall (SON) during 1979-2016. The boxes with white shading show a significant trend ($p < 0.1$). The cyclone density is based on the mean sea-level pressure fields from the reanalysis product ERA-Interim using an automated cyclone tracking algorithm. This figure is a modified version of Figure 2 in Paper I and is reprinted and modified with the permission of Wiley.

Paper II introduced a high-resolution operational NWP into the broader scope of our analyses. Given the uneven spatial distribution of the observational network in Svalbard, AROME-Arctic enabled us to study the local variability of the regional signals obtained from the composite analysis for the years 2013-2018. Although we acknowledge the short temporal extent of the AROME-Arctic period, this 5-year period is probably the best available representation of the present climate given the rapid environmental changes that have taken place over the last decades on Svalbard.

The “Niedźwiedź Classification” of atmospheric circulation patterns over Svalbard allowed us to systematically study the local seasonal sensitivity of 2-m air temperature, precipitation and rain-on-snow (ROS) to the geostrophic wind direction, which is indirectly controlled by the cyclone track. This work is the first to quantify ROS event frequencies and study their spatial extent in different atmospheric flow scenarios. ROS is defined in this work as DJF days with a mean daily 2-m air temperature above 0°C and 1 mm or more precipitation. We documented over 55 ROS events for 5 winter seasons, with 3% of the land grid points experiencing ROS (Figure 8a). These ROS events are the warmest and wettest in the southwestern parts of the archipelago (Figure 8 b,c). Our results suggest that sea ice explains a large part of the local variability in both 2-m air temperature and precipitation. Maybe not so surprising, most ROS events occur with southerly and southwesterly flow meaning that the cyclone track on average lies in the Fram Strait, a region with a positive trend in cyclone tracks (Paper I).

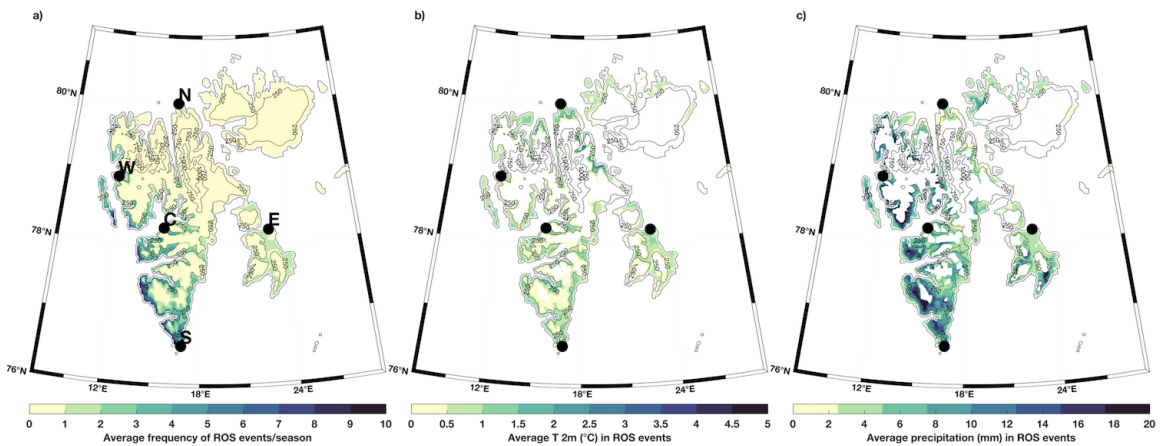


Figure 8) The average a) frequency, b) 2-m air temperature and c) precipitation in DJF rain-on-snow events during 2013-2018 in AROME-Arctic. This figure is a reprint of Figure 8 in Paper II with the permission from AGU.

Paper II demonstrates the local sensitivity of temperature and precipitation conditions to atmospheric circulation type. Paper III continues this work and incorporates analyses of change over time by employing the 11 km x 11 km gridded hindcast NORA10 over the 57 years between 1960-2017. As both Paper I and II in addition to the literature presented in this thesis find the largest changes in both time and space during winter, Paper III focuses solely on the extended winter season (NDJFM). A main finding of this study is the alarming near-surface air temperature trends of up to 3 K per decade in the northern and eastern parts of Svalbard - the areas that are not covered by the observational network (Figure 9c). The warming rates are only half of that in southern and western Svalbard, demonstrating the immense local gradient in wintertime warming. In addition to the temperature increase, large significant increases both in accumulated precipitation (+44.6 mm/decade) and the number of precipitation days (+5.2 days/decade) are reported in northern Svalbard (Figure 9a and b). A weaker, but still significant, trend in the number of precipitation (+1.3 days/decade) is found east of Svalbard. No significant precipitation changes are reported from the southern and western regions of Svalbard, further highlighting the

local variability of these climatic changes. Our results support the hypothesis of the changes in the north being attributed to sea ice losses north of Svalbard (Figure 9d).

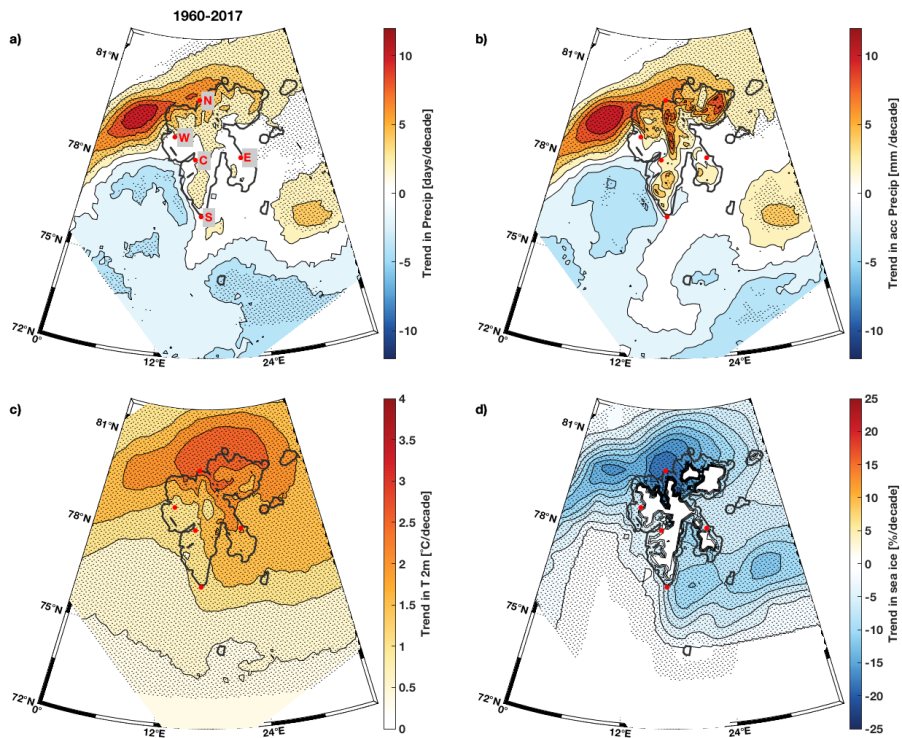


Figure 9) The trend in the extended winter (Nov-March) a) number of precipitation days, b) accumulated precipitation, c) 2-m air temperature and d) sea ice concentration per decade during 1960-2017 in the Norwegian hindcast model NOR10. The red dots represent automatic weather station locations that have been used to study the spatial variability in Papers II and III. This figure is a reprint of Figure 1 in Paper III with the permission of AGU.

In this thesis, my co-authors and I have advanced the regional and local scale understanding of winter season atmospheric circulation changes and their impacts on weather and climate in the high-latitude North Atlantic. We are the first to focus on the

effects and impacts of regional cyclone activity across a variety of spatial and temporal scales.

Furthermore, we have documented alarming winter temperature and precipitation increases in northern Svalbard, which demonstrate the consistently increasing heat content in this part of the Arctic and the unnerving speed at which these changes are occurring.

Future Perspectives

The number of new questions and interesting unknowns that have surfaced in the process of completing this doctoral thesis exceeds, by a wide margin, the questions answered. One of the most intriguing ones is the question of how to validate and deepen the process understanding behind the extreme rates of temperature and precipitation increase in the northern and eastern parts of the archipelago (Paper III).

There are studies showing that the grid size is crucial for cyclone tracking studies. Hence applying the tracking algorithm used in Paper I to the soon-to-be released reanalysis product based on AROME-Arctic, the NWP model used in Paper II, would be very interesting. This would also let one deepen one's understanding of the dynamics driving rain-on-snow events.

In the big picture, the Arctic keeps unequivocally warming for a number of years if not decades ahead, even if anthropogenic CO₂ emissions would cease this instance. We are moving towards a seasonally ice-free Arctic, and how this will affect atmospheric poleward heat transport remains uncertain. To date, climate projections have not found a consensus on how further warming is going to affect cyclone activity and alter atmospheric circulation in high latitudes. Among the main debates in the existing literature is the ‘tug-of-war’ between the surface-based warming in the Arctic and the upper tropospheric warming in the tropics. Along these lines the reduced meridional temperature gradient is acting to reduce cyclone activity and poleward transport of dry static heat, but on the other hand warmer air masses have the capacity to hold more moisture and can hence transport larger quantities of latent heat. To summarize, the question of how air, sea and ice interact in the future warm Arctic is not fully answered and inspires to continue and deepen the work initiated in this thesis.

References

- Aagaard, K., and P. Greisman, 1975: Toward new mass and heat budgets for the Arctic Ocean. *J. Geophys. Res.*, **80**, 3821–3827, <https://doi.org/10.1029/JC080i027p03821>.
- Hanssen-Bauer, I., and Coauthors, 2019: Climate in Svalbard 2100.
- Årthun, M., T. Eldevik, L. H. Smedsrud, Ø. Skagseth, and R. B. Ingvaldsen, 2012: Quantifying the Influence of Atlantic Heat on Barents Sea Ice Variability and Retreat. *J. Clim.*, **25**, 4736–4743, <https://doi.org/10.1175/JCLI-D-11-00466.1>.
- Barnes, E. A., and J. A. Screen, 2015: The impact of Arctic warming on the midlatitude jet-stream: Can it? Has it? Will it? *Wiley Interdisciplinary Reviews: Climate Change*, **6**, 277–286, <https://doi.org/10.1002/wcc.337>.
- Batrak, Y., E. Kourzeneva, and M. Homleid, 2018: Implementation of a simple thermodynamic sea ice scheme, SICE version 1.0-38h1, within the ALADIN–HIRLAM numerical weather prediction system version 38h1. *Geoscientific Model Development*, **11**, 3347–3368, <https://doi.org/10.5194/gmd-11-3347-2018>.
- Bengtsson, L., and Coauthors, 2017: The HARMONIE–AROME Model Configuration in the ALADIN–HIRLAM NWP System. *Mon. Weather Rev.*, **145**, 1919–1935, <https://doi.org/10.1175/MWR-D-16-0417.1>.
- Bintanja, R., R. G. Graversen, and W. Hazeleger, 2011: Arctic winter warming amplified by the thermal inversion and consequent low infrared cooling to space. *Nat. Geosci.*, **4**, 758–761, <https://doi.org/10.1038/ngeo1285>.
- Bjerknes, J., 1919: On the Structure of Moving Cyclones *Mon. Weather Rev.*, **47**, 95–99, <https://doi.org/2.0.CO;2> >10.1175/1520-0493(1919)47<95:OTSOMC>2.0.CO;2.
- Boisvert, L. N., A. A. Petty, and J. C. Stroeve, 2016: The Impact of the Extreme Winter 2015/16 Arctic Cyclone on the Barents–Kara Seas. *Mon. Weather Rev.*, **144**, 4279–4287, <https://doi.org/10.1175/MWR-D-16-0234.1>.
- Brayshaw, D. J., B. Hoskins, and M. Blackburn, 2009: The Basic Ingredients of the North Atlantic Storm Track. Part I: Land–Sea Contrast and Orography. *J. Atmos. Sci.*, **66**, 2539–2558, <https://doi.org/10.1175/2009JAS3078.1>.
- , ———, and ———, 2011: The Basic Ingredients of the North Atlantic Storm Track. Part II: Sea Surface Temperatures. *J. Atmos. Sci.*, **68**, 1784–1805, <https://doi.org/10.1175/2011JAS3674.1>.
- Breivik, Ø., O. J. Aarnes, J.-R. Bidlot, A. Carrasco, and Ø. Sætra, 2013: Wave Extremes in the Northeast Atlantic from Ensemble Forecasts. *J. Clim.*, **26**, 7525–7540, <https://doi.org/10.1175/JCLI-D-12-00738.1>.
- Butler, A. H., D. W. J. Thompson, and R. Heikes, 2010: The Steady-State Atmospheric Circulation Response to Climate Change–like Thermal Forcings in a Simple General Circulation Model. *J. Clim.*, **23**, 3474–3496, <https://doi.org/10.1175/2010JCLI3228.1>.
- Cai, M., 2005: Dynamical amplification of polar warming. *Geophys. Res. Lett.*, **32**, <https://doi.org/10.1029/2005GL024481>.
- Carmack, E., and Coauthors, 2015: Toward Quantifying the Increasing Role of Oceanic Heat in Sea Ice Loss in the New Arctic. *Bull. Am. Meteorol. Soc.*, **96**, 2079–2105, <https://doi.org/10.1175/BAMS-D-13-00177.1>.

- Chang, E. K. M., Y. Guo, and X. Xia, 2012: CMIP5 multimodel ensemble projection of storm track change under global warming. *J. Geophys. Res. D: Atmos.*, **117**.
- Charney, J. G., 1947: The Dynamics of Long Waves in a baroclinic Westerly Current. *J. Meteorol.*, **4**, 136–162, <https://doi.org/2.0.CO;2>>10.1175/1520-0469(1947)004<0136:TDOLWI>2.0.CO;2.
- Chylek, P., C. K. Folland, G. Lesins, M. K. Dubey, and M. Wang, 2009: Arctic air temperature change amplification and the Atlantic Multidecadal Oscillation. *Geophys. Res. Lett.*, **36**, 2721, <https://doi.org/10.1029/2009GL038777>.
- Cohen, J., and Coauthors, 2014: Recent Arctic amplification and extreme mid-latitude weather. *Nat. Geosci.*, **7**, 627–637, <https://doi.org/10.1038/ngeo2234>.
- Cohen, J., and Coauthors, 2019: Divergent consensus on Arctic amplification influence on midlatitude severe winter weather. *Nat. Clim. Chang.*, **10**, 20–29, <https://doi.org/10.1038/s41558-019-0662-y>.
- Collins, M., and Coauthors, 2018: Challenges and opportunities for improved understanding of regional climate dynamics. *Nat. Clim. Chang.*, **8**, 101–108, <https://doi.org/10.1038/s41558-017-0059-8>.
- Cottier, F. R., F. Nilsen, M. E. Inall, S. Gerland, V. Tverberg, and H. Svendsen, 2007: Wintertime warming of an Arctic shelf in response to large-scale atmospheric circulation. *Geophys. Res. Lett.*, **34**.
- Crawford, A. D., and M. C. Serreze, 2016: Does the Summer Arctic Frontal Zone Influence Arctic Ocean Cyclone Activity? *J. Clim.*, **29**, 4977–4993, <https://doi.org/10.1175/JCLI-D-15-0755.1>.
- Dacre, H. F., M. K. Hawcroft, M. A. Stringer, and K. I. Hodges, 2012: An Extratropical Cyclone Atlas: A Tool for Illustrating Cyclone Structure and Evolution Characteristics. *Bull. Am. Meteorol. Soc.*, **93**, 1497–1502, <https://doi.org/10.1175/BAMS-D-11-00164.1>.
- Dai, A., D. Luo, M. Song, and J. Liu, 2019: Arctic amplification is caused by sea-ice loss under increasing CO₂. *Nat. Commun.*, **10**, 121, <https://doi.org/10.1038/s41467-018-07954-9>.
- Dee, D. P., and Coauthors, 2011: The ERA-Interim reanalysis: configuration and performance of the data assimilation system. *Quarterly Journal of the Royal Meteorological Society*, **137**, 553–597, <https://doi.org/10.1002/qj.828>.
- Deser, C., A. Phillips, V. Bourdette, and H. Teng, 2012: Uncertainty in climate change projections: the role of internal variability. *Clim. Dyn.*, **38**, 527–546, <https://doi.org/10.1007/s00382-010-0977-x>.
- , R. A. Tomas, and L. Sun, 2015: The Role of Ocean–Atmosphere Coupling in the Zonal-Mean Atmospheric Response to Arctic Sea Ice Loss. *J. Clim.*, **28**, 2168–2186, <https://doi.org/10.1175/JCLI-D-14-00325.1>.
- , L. Sun, R. A. Tomas, and J. Screen, 2017: Does ocean coupling matter for the northern extratropical response to projected Arctic sea ice loss? *Geophys. Res. Lett.*, 2149–2157, <https://doi.org/10.1002/2016GL067792>@10.1002/(ISSN)1944-8007.ATMOSLINKAGES1.
- Ding, Q., J. M. Wallace, D. S. Battisti, E. J. Steig, A. J. E. Gallant, H.-J. Kim, and L. Geng, 2014: Tropical forcing of the recent rapid Arctic warming in northeastern Canada and Greenland. *Nature*, **509**, 209–212, <https://doi.org/10.1038/nature13260>.

- Donlon, C. J., M. Martin, J. Stark, J. Roberts-Jones, E. Fiedler, and W. Wimmer, 2012: The Operational Sea Surface Temperature and Sea Ice Analysis (OSTIA) system. *Remote Sens. Environ.*, **116**, 140–158, <https://doi.org/10.1016/j.rse.2010.10.017>.
- Dufour, A., O. Zolina, and S. K. Gulev, 2016: Atmospheric Moisture Transport to the Arctic: Assessment of Reanalyses and Analysis of Transport Components. *J. Clim.*, **29**, 5061–5081, <https://doi.org/10.1175/JCLI-D-15-0559.1>.
- Eady, E. T., 1949: Long Waves and Cyclone Waves. *Tell'Us*, **1**, 33–52, <https://doi.org/10.3402/tellusa.v1i3.8507>.
- Francis, J. A., S. J. Vavrus, and J. Cohen, 2017: Amplified Arctic warming and mid-latitude weather: new perspectives on emerging connections. *Wiley Interdisciplinary Reviews: Climate Change*, **8**, e474, <https://doi.org/10.1002/wcc.474>.
- Gill, A. E., 2016: *Atmosphere—Ocean Dynamics*. Elsevier, 682 pp.
- Gong, T., S. Feldstein, and S. Lee, 2017: The Role of Downward Infrared Radiation in the Recent Arctic Winter Warming Trend. *J. Clim.*, **30**, 4937–4949, <https://doi.org/10.1175/JCLI-D-16-0180.1>.
- Graff, L. S., and J. H. LaCasce, 2014: Changes in Cyclone Characteristics in Response to Modified SSTs. *J. Clim.*, **27**, 4273–4295, <https://doi.org/10.1175/JCLI-D-13-00353.1>.
- Graham, R. M., L. Cohen, A. A. Petty, L. N. Boisvert, A. Rinke, S. R. Hudson, M. Nicolaus, and M. A. Granskog, 2017: Increasing frequency and duration of Arctic winter warming events. *Geophys. Res. Lett.*, **44**, 6974–6983, <https://doi.org/10.1002/2017GL073395>.
- , and Coauthors, 2019: Winter storms accelerate the demise of sea ice in the Atlantic sector of the Arctic Ocean. *Sci. Rep.*, **9**, 9222, <https://doi.org/10.1038/s41598-019-45574-5>.
- Graversen, R. G., T. Mauritsen, M. Tjernström, E. Källén, and G. Svensson, 2008: Vertical structure of recent Arctic warming. *Nature*, **451**, 53–56, <https://doi.org/10.1038/nature06502>.
- Hall, R., R. Erdélyi, E. Hanna, J. M. Jones, and A. A. Scaife, 2015: Drivers of North Atlantic Polar Front jet stream variability. *Int. J. Climatol.*, **35**, 1697–1720, <https://doi.org/10.1002/joc.4121>.
- Hancock, H., A. Prokop, M. Eckerstorfer, and J. Hendrikx, 2018: Combining high spatial resolution snow mapping and meteorological analyses to improve forecasting of destructive avalanches in Longyearbyen, Svalbard. *Cold Reg. Sci. Technol.*, **154**, 120–132, <https://doi.org/10.1016/j.coldregions.2018.05.011>.
- Hansen, B. B., and Coauthors, 2019: More frequent extreme climate events stabilize reindeer population dynamics. *Nat. Commun.*, **10**, 1616, <https://doi.org/10.1038/s41467-019-09332-5>.
- Held, I. M., and A. Y. Hou, 1980: Nonlinear Axially Symmetric Circulations in a Nearly Inviscid Atmosphere. *J. Atmos. Sci.*, **37**, 515–533, [https://doi.org/10.1175/1520-0469\(1980\)037<0515:NASCIA>2.0.CO;2](https://doi.org/10.1175/1520-0469(1980)037<0515:NASCIA>2.0.CO;2).
- Hewson, T. D., G. C. Craig, and C. Claud, 2000: Evolution and mesoscale structure of a polar low outbreak. *Quart. J. Roy. Meteor. Soc.*, **126**, 1031–1063.
- Hodges, K. I., B. J. Hoskins, J. Boyle, and C. Thorncroft, 2003: A Comparison of Recent Reanalysis Datasets Using Objective Feature Tracking: Storm Tracks and Tropical Easterly Waves. *Monthly Weather Review*, **131**, 2012–2037, [https://doi.org/10.1175/1520-0493\(2003\)131<2012:acorrd>2.0.co;2](https://doi.org/10.1175/1520-0493(2003)131<2012:acorrd>2.0.co;2).

- Holton, J. R., 1973: An Introduction to Dynamic Meteorology. *Am. J. Phys.*, **41**, 752–754, <https://doi.org/10.1119/1.1987371>.
- Hoskins, B. J., and K. I. Hodges, 2002: New Perspectives on the Northern Hemisphere Winter Storm Tracks. *J. Atmos. Sci.*, **59**, 1041–1061, <https://doi.org/2.0.CO;2>>10.1175/1520-0469(2002)059<1041:NPOTNH>2.0.CO;2.
- , I. N. James, and G. H. White, 1983: The Shape, Propagation and Mean-Flow Interaction of Large-Scale Weather Systems. *J. Atmos. Sci.*, **40**, 1595–1612, <https://doi.org/2.0.CO;2>>10.1175/1520-0469(1983)040<1595:TSPAMF>2.0.CO;2.
- Isaksen, K., Ø. Nordli, E. J. Førland, E. Łupikasza, S. Eastwood, and T. Niedźwiedz, 2016: Recent warming on Spitsbergen-Influence of atmospheric circulation and sea ice cover. *J. Geophys. Res. D: Atmos.*, **121**, 11,913–11,931, <https://doi.org/10.1002/2016JD025606>.
- Kashiwase, H., K. I. Ohshima, S. Nishashi, and H. Eicken, 2017: Evidence for ice-ocean albedo feedback in the Arctic Ocean shifting to a seasonal ice zone. *Scientific Reports*, **7**, <https://doi.org/10.1038/s41598-017-08467-z>.
- Kim, B.-M., S.-W. Son, S.-K. Min, J.-H. Jeong, S.-J. Kim, X. Zhang, T. Shim, and J.-H. Yoon, 2014: Weakening of the stratospheric polar vortex by Arctic sea-ice loss. *Nat. Commun.*, **5**, 4646, <https://doi.org/10.1038/ncomms5646>.
- , and Coauthors, 2017: Major cause of unprecedented Arctic warming in January 2016: Critical role of an Atlantic windstorm. *Sci. Rep.*, **7**, 40051, <https://doi.org/10.1038/srep40051>.
- Kim, K.-Y., J.-Y. Kim, J. Kim, S. Yeo, H. Na, B. D. Hamlington, and R. R. Leben, 2019: Vertical Feedback Mechanism of Winter Arctic Amplification and Sea Ice Loss. *Sci. Rep.*, **9**, 1184, <https://doi.org/10.1038/s41598-018-38109-x>.
- King, J., G. Spreen, S. Gerland, C. Haas, S. Hendricks, L. Kaleschke, and C. Wang, 2017: Sea-ice thickness from field measurements in the northwestern Barents Sea. *Journal of Geophysical Research: Oceans*, **122**, 1497–1512, <https://doi.org/10.1002/2016jc012199>.
- Køltzow, M., B. Casati, E. Bazile, T. Haiden, and T. Valkonen, 2019: An NWP Model Intercomparison of Surface Weather Parameters in the European Arctic during the Year of Polar Prediction Special Observing Period Northern Hemisphere 1. *Weather Forecast.*, **34**, 959–983, <https://doi.org/10.1175/WAF-D-19-0003.1>.
- Koyama, T., J. Stroeve, J. Cassano, and A. Crawford, 2017: Sea Ice Loss and Arctic Cyclone Activity from 1979 to 2014. *J. Clim.*, **30**, 4735–4754, <https://doi.org/10.1175/JCLI-D-16-0542.1>.
- Lamb, H. H., 1972: British Isles weather types and a register of the daily sequence of circulation patterns 1861-1971.
- Lee, S., and H.-K. Kim, 2003: The Dynamical Relationship between Subtropical and Eddy-Driven Jets. *J. Atmos. Sci.*, **60**, 1490–1503, <https://doi.org/2.0.CO;2>>10.1175/1520-0469(2003)060<1490:TDRBSA>2.0.CO;2.
- Luo, B., L. Wu, D. Luo, A. Dai, and I. Simmonds, 2019: The winter midlatitude-Arctic interaction: effects of North Atlantic SST and high-latitude blocking on Arctic sea ice and Eurasian cooling. *Clim. Dyn.*, **52**, 2981–3004, <https://doi.org/10.1007/s00382-018-4301-5>.
- Lynch, A. H., A. H. Lynch, and J. J. Cassano, 2006: *Applied Atmospheric Dynamics*. Wiley, 280 pp.
- Mäkiranta, E., T. Vihma, A. Sjöblom, and E.-M. Tastula, 2011: Observations and Modelling of the Atmospheric Boundary Layer Over Sea-Ice in a Svalbard Fjord. *Bound.-Layer Meteorol.*, **140**,

105, <https://doi.org/10.1007/s10546-011-9609-1>.

- Marshall, J., K. C. Armour, J. R. Scott, Y. Kostov, U. Hausmann, D. Ferreira, T. G. Shepherd, and C. M. Bitz, 2014: The ocean's role in polar climate change: asymmetric Arctic and Antarctic responses to greenhouse gas and ozone forcing. *Philos. Trans. A Math. Phys. Eng. Sci.*, **372**, 20130040, <https://doi.org/10.1098/rsta.2013.0040>.
- McCusker, K. E., P. J. Kushner, J. C. Fyfe, M. Sigmond, V. V. Kharin, and C. M. Bitz, 2017: Remarkable separability of circulation response to Arctic sea ice loss and greenhouse gas forcing. *Geophys. Res. Lett.*, **44**, 7955–7964.
- Minobe, S., M. Miyashita, A. Kuwano-Yoshida, H. Tokinaga, and S.-P. Xie, 2010: Atmospheric Response to the Gulf Stream: Seasonal Variations. *J. Clim.*, **23**, 3699–3719, <https://doi.org/10.1175/2010JCLI3359.1>.
- Muckenhuber, S., F. Nilsen, A. Korosov, and S. Sandven, 2016: Sea ice cover in Isfjorden and Hornsund, Svalbard (2000–2014) from remote sensing data. *The Cryosphere*, **10**, 149–158, <https://doi.org/10.5194/tc-10-149-2016>.
- Müller, M., Y. Batrak, J. Kristiansen, M. A. Ø. Køltzow, G. Noer, and A. Korosov, 2017: Characteristics of a Convective-Scale Weather Forecasting System for the European Arctic. *Mon. Weather Rev.*, **145**, 4771–4787, <https://doi.org/10.1175/MWR-D-17-0194.1>.
- Murray, R. J., and I. Simmonds, 1991: A numerical scheme for tracking cyclone centres from digital data. Part I: Development and operation of the scheme. *Aust. Meteorol. Mag.*, **39**, 155–166.
- Naakka, T., T. Nygård, and T. Vihma, 2018: Arctic Humidity Inversions: Climatology and Processes. *J. Clim.*, **31**, 3765–3787, <https://doi.org/10.1175/JCLI-D-17-0497.1>.
- , ———, ———, J. Sedlar, and R. Graversen, 2019: Atmospheric moisture transport between mid-latitudes and the Arctic: Regional, seasonal and vertical distributions. *Int. J. Climatol.*, **39**, 2862–2879, <https://doi.org/10.1002/joc.5988>.
- Nakamura, T., K. Yamazaki, K. Iwamoto, M. Honda, Y. Miyoshi, Y. Ogawa, and J. Ukita, 2015: A negative phase shift of the winter AO/NAO due to the recent Arctic sea-ice reduction in late autumn. *Journal of Geophysical Research: Atmospheres*, **120**, 3209–3227, <https://doi.org/10.1002/2014jd022848>.
- , ———, ———, ———, ———, ———, Y. Tomikawa, and J. Ukita, 2016: The stratospheric pathway for Arctic impacts on midlatitude climate. *Geophys. Res. Lett.*, **43**, 3494–3501, <https://doi.org/10.1002/2016GL068330>.
- Neu, U., and Coauthors, 2013: IMILAST: A Community Effort to Intercompare Extratropical Cyclone Detection and Tracking Algorithms. *Bull. Am. Meteorol. Soc.*, **94**, 529–547, <https://doi.org/10.1175/BAMS-D-11-00154.1>.
- Nilsen, F., R. Skogseth, J. Vaardal-Lunde, and M. Inall, 2016: A Simple Shelf Circulation Model: Intrusion of Atlantic Water on the West Spitsbergen Shelf. *J. Phys. Oceanogr.*, **46**, 1209–1230, <https://doi.org/10.1175/JPO-D-15-0058.1>.
- Nygård, T., R. G. Graversen, P. Uotila, T. Naakka, and T. Vihma, 2019: Strong Dependence of Wintertime Arctic Moisture and Cloud Distributions on Atmospheric Large-Scale Circulation. *Journal of Climate*, **32**, 8771–8790, <https://doi.org/10.1175/jcli-d-19-0242.1>.
- Onarheim, I. H., L. H. Smedsrud, R. B. Ingvaldsen, and F. Nilsen, 2014: Loss of sea ice during winter north of Svalbard. *Tellus A: Dynamic Meteorology and Oceanography*, **66**, 23933, <https://doi.org/10.3402/tellusa.v66.23933>.

- , T. Eldevik, L. H. Smedsrud, and J. C. Stroeve, 2018: Seasonal and Regional Manifestation of Arctic Sea Ice Loss. *J. Clim.*, **31**, 4917–4932, <https://doi.org/10.1175/JCLI-D-17-0427.1>.
- Panetta, R. L., and I. M. Held, 1988: Baroclinic Eddy Fluxes in a One-Dimensional Model of Quasi-geostrophic Turbulence. *J. Atmos. Sci.*, **45**, 3354–3365, [https://doi.org/10.1175/1520-0469\(1988\)045<3354:BEFIAO>2.0.CO;2](https://doi.org/10.1175/1520-0469(1988)045<3354:BEFIAO>2.0.CO;2).
- Parding, K. M., R. Benestad, A. Mezghani, and H. B. Erlandsen, 2019: Statistical Projection of the North Atlantic Storm Tracks. *J. Appl. Meteorol. Climatol.*, **58**, 1509–1522, <https://doi.org/10.1175/JAMC-D-17-0348.1>.
- Park, H.-S., S. Lee, S.-W. Son, S. B. Feldstein, and Y. Kosaka, 2015: The Impact of Poleward Moisture and Sensible Heat Flux on Arctic Winter Sea Ice Variability. *J. Clim.*, **28**, 5030–5040, <https://doi.org/10.1175/JCLI-D-15-0074.1>.
- Petterssen, S., 1957: Weather Observations, Analysis, and Forecasting. *Meteorological Research Reviews: Summaries of Progress from 1951 to 1955*, H.E. Landsberg et al., Eds., American Meteorological Society, 114–151.
- Pithan, F., and T. Mauritsen, 2014: Arctic amplification dominated by temperature feedbacks in contemporary climate models. *Nat. Geosci.*, **7**, 181, <https://doi.org/10.1038/ngeo2071>.
- Raible, C. C., B. Ziv, H. Saaroni, and M. Wild, 2010: Winter synoptic-scale variability over the Mediterranean Basin under future climate conditions as simulated by the ECHAM5. *Clim. Dyn.*, **35**, 473–488, <https://doi.org/10.1007/s00382-009-0678-5>.
- Reed, R. J., 1990: Advances in Knowledge and Understanding of Extratropical Cyclones during the Past Quarter Century: An Overview. *Extratropical Cyclones: The Erik Palmén Memorial Volume*, C.W. Newton and E.O. Holopainen, Eds., American Meteorological Society, 27–45.
- Reistad, M., Ø. Breivik, H. Haakenstad, O. J. Aarnes, B. R. Furevik, and J.-R. Bidlot, 2011: A high-resolution hindcast of wind and waves for the North Sea, the Norwegian Sea, and the Barents Sea. *J. Geophys. Res. C: Oceans*, **116**.
- Rinke, A., M. Maturilli, R. M. Graham, H. Matthes, D. Handorf, L. Cohen, S. R. Hudson, and J. C. Moore, 2017: Extreme cyclone events in the Arctic: Wintertime variability and trends. *Environ. Res. Lett.*, **12**, 094006, <https://doi.org/10.1088/1748-9326/aa7def>.
- , and Coauthors, 2019: Trends of Vertically Integrated Water Vapor over the Arctic during 1979–2016: Consistent Moistening All Over? *J. Clim.*, **32**, 6097–6116, <https://doi.org/10.1175/JCLI-D-19-0092.1>.
- Rosby, C. G., 1939: Planetary flow patterns in the atmosphere. *Quart. J. Roy. Meteor. Soc.*, **66**, 68.
- Rudeva, I., and S. K. Gulev, 2007: Climatology of Cyclone Size Characteristics and Their Changes during the Cyclone Life Cycle. *Mon. Weather Rev.*, **135**, 2568–2587, <https://doi.org/10.1175/MWR3420.1>.
- , and I. Simmonds, 2015: Variability and Trends of Global Atmospheric Frontal Activity and Links with Large-Scale Modes of Variability. *J. Clim.*, **28**, 3311–3330, <https://doi.org/10.1175/JCLI-D-14-00458.1>.
- Schlichtholz, P., 2018: Climate impacts and Arctic precursors of changing storm track activity in the Atlantic-Eurasian region. *Sci. Rep.*, **8**, 17786, <https://doi.org/10.1038/s41598-018-35900-8>.
- Screen, J. A., and I. Simmonds, 2010a: Increasing fall-winter energy loss from the Arctic Ocean and its role in Arctic temperature amplification. *Geophys. Res. Lett.*,

- Screen, J. A., and I. Simmonds, 2010b: The central role of diminishing sea ice in recent Arctic temperature amplification. *Nature*, **464**, 1334–1337, <https://doi.org/10.1038/nature09051>.
- , and J. A. Francis, 2016: Contribution of sea-ice loss to Arctic amplification is regulated by Pacific Ocean decadal variability. *Nat. Clim. Chang.*, **6**, 856–860, <https://doi.org/10.1038/nclimate3011>.
- , I. Simmonds, C. Deser, and R. Tomas, 2013: The Atmospheric Response to Three Decades of Observed Arctic Sea Ice Loss. *J. Clim.*, **26**, 1230–1248, <https://doi.org/10.1175/JCLI-D-12-00063.1>.
- , C. Deser, I. Simmonds, and R. Tomas, 2014: Atmospheric impacts of Arctic sea-ice loss, 1979–2009: separating forced change from atmospheric internal variability. *Clim. Dyn.*, **43**, 333–344, <https://doi.org/10.1007/s00382-013-1830-9>.
- , and Coauthors, 2018a: Consistency and discrepancy in the atmospheric response to Arctic sea-ice loss across climate models. *Nat. Geosci.*, **11**, 155–163, <https://doi.org/10.1038/s41561-018-0059-y>.
- Screen, J. A., T. J. Bracegirdle, and I. Simmonds, 2018b: Polar Climate Change as Manifest in Atmospheric Circulation. *Curr Clim Change Rep*, **4**, 383–395, <https://doi.org/10.1007/s40641-018-0111-4>.
- Sepp, M., and J. Jaagus, 2011: Changes in the activity and tracks of Arctic cyclones. *Clim. Change*, **105**, 577–595, <https://doi.org/10.1007/s10584-010-9893-7>.
- Serebreny, S. M., E. J. Wiegman, and R. G. Hadfield, 1962: Some Characteristic Features of the Jet Stream Complex during Selected Synoptic Conditions. *J. Appl. Meteorol.*, **1**, 137–153, [https://doi.org/2.0.CO;2">10.1175/1520-0450\(1962\)001<0137:SCFOTJ>2.0.CO;2](https://doi.org/2.0.CO;2).
- Serreze, M. C., and A. P. Barrett, 2008: The Summer Cyclone Maximum over the Central Arctic Ocean. *J. Clim.*, **21**, 1048–1065, <https://doi.org/10.1175/2007JCLI1810.1>.
- , and R. G. Barry, 2014: *The Arctic Climate System*. Cambridge University Press, 404 pp.
- Serreze, M. C., A. P. Barrett, J. C. Stroeve, D. N. Kindig, and M. M. Holland, 2008: The emergence of surface-based Arctic amplification. *The Cryosphere Discussions*, **2**, 601–622, <https://doi.org/10.5194/tcd-2-601-2008>.
- Shaw, T. A., and Coauthors, 2016: Storm track processes and the opposing influences of climate change. *Nat. Geosci.*, **9**, 656–664, <https://doi.org/10.1038/ngeo2783>.
- Shepherd, T. G., 2014: Atmospheric circulation as a source of uncertainty in climate change projections. *Nat. Geosci.*, **7**, 703–708, <https://doi.org/10.1038/ngeo2253>.
- Simmonds, I., and E.-P. Lim, 2009: Biases in the calculation of Southern Hemisphere mean baroclinic eddy growth rate. *Geophys. Res. Lett.*, **36**, 115, <https://doi.org/10.1029/2008GL036320>.
- , and I. Rudeva, 2012: The great Arctic cyclone of August 2012. *Geophys. Res. Lett.*, **39**, <https://doi.org/10.1029/2012GL054259>.
- , and ———, 2014: A comparison of tracking methods for extreme cyclones in the Arctic basin. *Tellus Ser. A Dyn. Meteorol. Oceanogr.*, **66**, 25252, <https://doi.org/10.3402/tellusa.v66.25252>.
- , C. Burke, and K. Keay, 2008: Arctic Climate Change as Manifest in Cyclone Behavior. *J. Clim.*, **21**, 5777–5796, <https://doi.org/10.1175/2008JCLI2366.1>.

- Sinclair, M. R., 1994: An Objective Cyclone Climatology for the Southern Hemisphere. *Mon. Weather Rev.*, **122**, 2239–2256, <https://doi.org/2.0.CO;2>>10.1175/1520-0493(1994)122<2239:AOCFFT>2.0.CO;2.
- Smedsrud, L. H., and Coauthors, 2013: The Role of Barents Sea in the Arctic Climate System *Rev. Geophys.*, **51**, 415–449, <https://doi.org/10.1002/rog.20017>.
- Smith, D. M., N. J. Dunstone, A. A. Scaife, E. K. Fiedler, D. Copsey, and S. C. Hardiman, 2017: Atmospheric Response to Arctic and Antarctic Sea Ice: The Importance of Ocean–Atmosphere Coupling and the Background State. *J. Clim.*, **30**, 4547–4565, <https://doi.org/10.1175/JCLI-D-16-0564.1>.
- Sorteberg, A., and J. E. Walsh, 2008: Seasonal cyclone variability at 70°N and its impact on moisture transport into the Arctic. *Tellus A*, **60**, 570–586, <https://doi.org/10.1111/j.1600-0870.2008.00314.x>.
- Spielhagen, R. F., and Coauthors, 2011: Enhanced modern heat transfer to the Arctic by warm Atlantic Water. *Science*, **331**, 450–453, <https://doi.org/10.1126/science.1197397>.
- Stroeve, J., and D. Notz, 2018: Changing state of Arctic sea ice across all seasons. *Environ. Res. Lett.*, **13**, 103001, <https://doi.org/10.1088/1748-9326/aade56>.
- Sun, L., C. Deser, and R. A. Tomas, 2015: Mechanisms of Stratospheric and Tropospheric Circulation Response to Projected Arctic Sea Ice Loss. *J. Clim.*, **28**, 7824–7845, <https://doi.org/10.1175/JCLI-D-15-0169.1>.
- Tamarin, T., and Y. Kaspi, 2017: The poleward shift of storm tracks under global warming: A Lagrangian perspective. *Geophys. Res. Lett.*, **44**, 10,666–10,674, <https://doi.org/10.1002/2017GL073633>.
- Tang, Q., X. Zhang, X. Yang, and J. A. Francis, 2013: Cold winter extremes in northern continents linked to Arctic sea ice loss. *Environ. Res. Lett.*, **8**, 014036, <https://doi.org/10.1088/1748-9326/8/1/014036>.
- Thackeray, C. W., and A. Hall, 2019: An emergent constraint on future Arctic sea-ice albedo feedback. *Nat. Clim. Chang.*, **9**, 972–978, <https://doi.org/10.1038/s41558-019-0619-1>.
- Thompson, D. W. J., and J. M. Wallace, 2000: Annular Modes in the Extratropical Circulation. Part I: Month-to-Month Variability. *J. Clim.*, **13**, 1000–1016, <https://doi.org/2.0.CO;2>>10.1175/1520-0442(2000)013<1000:AMITEC>2.0.CO;2.
- Turner, J., J. E. Overland, and J. E. Walsh, 2007: An Arctic and antarctic perspective on recent climate change. *Int. J. Climatol.*, **27**, 277–293, <https://doi.org/10.1002/joc.1406>.
- Ulbrich, U., G. C. Leckebusch, and J. G. Pinto, 2009: Extra-tropical cyclones in the present and future climate: a review. *Theor. Appl. Climatol.*, **96**, 117–131, <https://doi.org/10.1007/s00704-008-0083-8>.
- Undén, P., and Coauthors, 2002: HIRLAM-5 scientific documentation.
- Uppala, S. M., and Coauthors, 2005: The ERA-40 re-analysis. *Q.J.R. Meteorol. Soc.*, **131**, 2961–3012, <https://doi.org/10.1256/qj.04.176>.
- Vallis, G. K., and E. P. Gerber, 2008: Local and hemispheric dynamics of the North Atlantic Oscillation, annular patterns and the zonal index. *Dyn. Atmos. Oceans*, **44**, 184–212, <https://doi.org/10.1016/j.dynatmoce.2007.04.003>.

- Vavrus, S. J., 2013: Extreme Arctic cyclones in CMIP5 historical simulations. *Geophys. Res. Lett.*, **40**, 6208–6212.
- Vihma, T., 2014: Effects of Arctic Sea Ice Decline on Weather and Climate: A Review. *Surveys in Geophysics*, **35**, 1175–1214, <https://doi.org/10.1007/s10712-014-9284-0>.
- Vihma, T., J. Screen, and M. Tjernström, 2016: The atmospheric role in the Arctic water cycle: A review on processes, past and future changes, and their impacts. *Journal of*.
- Vikhamar-Schuler, D., K. Isaksen, J. E. Haugen, H. Tømmervik, B. Luks, T. V. Schuler, and J. W. Bjerke, 2016: Changes in Winter Warming Events in the Nordic Arctic Region. *J. Clim.*, **29**, 6223–6244, <https://doi.org/10.1175/JCLI-D-15-0763.1>.
- Walsh, J. E., 2014: Intensified warming of the Arctic: Causes and impacts on middle latitudes. *Glob. Planet. Change*, **117**, 52–63, <https://doi.org/10.1016/j.gloplacha.2014.03.003>.
- Wei, L., T. Qin, and C. Li, 2017: Seasonal and inter-annual variations of Arctic cyclones and their linkage with Arctic sea ice and atmospheric teleconnections. *Acta Oceanol. Sin.*, **36**, 1–7, <https://doi.org/10.1007/s13131-017-1117-9>.
- Woods, C., and R. Caballero, 2016: The Role of Moist Intrusions in Winter Arctic Warming and Sea Ice Decline. *J. Clim.*, **29**, 4473–4485, <https://doi.org/10.1175/JCLI-D-15-0773.1>.
- Woollings, T., J. M. Gregory, J. G. Pinto, M. Reyers, and D. J. Brayshaw, 2012: Response of the North Atlantic storm track to climate change shaped by ocean–atmosphere coupling. *Nat. Geosci.*, **5**, 313–317, <https://doi.org/10.1038/ngeo1438>.
- Wu, Y., and K. L. Smith, 2016: Response of Northern Hemisphere Midlatitude Circulation to Arctic Amplification in a Simple Atmospheric General Circulation Model. *J. Clim.*, **29**, 2041–2058, <https://doi.org/10.1175/JCLI-D-15-0602.1>.
- Yang, X.-Y., X. Yuan, and M. Ting, 2016: Dynamical Link between the Barents–Kara Sea Ice and the Arctic Oscillation. *J. Clim.*, **29**, 5103–5122, <https://doi.org/10.1175/JCLI-D-15-0669.1>.
- Yin, J. H., 2005: A consistent poleward shift of the storm tracks in simulations of 21st century climate. *Geophys. Res. Lett.*,
- Zahn, M., M. Akperov, A. Rinke, F. Feser, and I. I. Mokhov, 2018: Trends of Cyclone Characteristics in the Arctic and Their Patterns From Different Reanalysis Data. *J. Geophys. Res. D: Atmos.*, **123**, 2737–2751, <https://doi.org/10.1002/2017JD027439>.
- Zhang, X., J. E. Walsh, J. Zhang, U. S. Bhatt, and M. Ikeda, 2004: Climatology and Interannual Variability of Arctic Cyclone Activity: 1948–2002. *J. Clim.*, **17**, 2300–2317, [https://doi.org/10.1175/1520-0442\(2004\)017<2300:CAIVOA>2.0.CO;2](https://doi.org/10.1175/1520-0442(2004)017<2300:CAIVOA>2.0.CO;2).
- , A. Sorteberg, J. Zhang, R. Gerdes, and J. C. Comiso, 2008: Recent radical shifts of atmospheric circulations and rapid changes in Arctic climate system. *Geophys. Res. Lett.*, **35**, L01703, <https://doi.org/10.1029/2008GL035607>.
- , J. He, J. Zhang, I. Polyakov, R. Gerdes, J. Inoue, and P. Wu, 2013: Enhanced poleward moisture transport and amplified northern high-latitude wetting trend. *Nat. Clim. Chang.*, **3**, 47–51, <https://doi.org/10.1038/nclimate1631>.
- Bjerknes, J., and H. Solberg, 1922: Life cycle of cyclones and the polar front theory of atmospheric circulation. *Geophys. Publ.*, **3** (1), 3–18, http://www.ngfweb.no/docs/NGF_GP_Vol03_no1.pdf
- NOAA National Centers for Environmental Information, State of the Climate: Global Climate Report

for Annual 2019, published online January 2020, retrieved on February 22, 2020 from <https://www.ncdc.noaa.gov/sotc/global/201913>.

Hess P, Brezowsky H (1952) Katalog der Grosswetterlagen Europas. Berichte des Deutschen Wetterdienstes in der US-Zone, 33

Hess P, Brezowsky H (1969) Katalog der Grosswetterlagen Europas, 2. neu bearbeitete und ergänzte Aufl. Berichte des Deutschen Wetterdienstes 113. Offenbach am Main


Hess P, Brezowsky H (1977) Katalog der Grosswetterlagen Europas 1881–1976, 3. verbesserte und ergänzte Aufl. Berichte des Deutschen Wetterdienstes 113. Offenbach am Main

Niedźwiedz, T. (2013), The atmospheric circulation, in Climate and Climate Change at Hornsund, Svalbard, edited by A. A. Marsz and A. Styszyńska, pp. 57–74, Gdynia Maritime Univ., Gdynia, Poland.

Paper I

RESEARCH ARTICLE

Trends in cyclones in the high-latitude North Atlantic during 1979–2016

S. Wickström^{1,2}  | M. O. Jonassen^{1,2} | T. Vihma^{1,3} | P. Uotila⁴

¹Department of Arctic Geophysics, The University Centre in Svalbard, Longyearbyen, Norway

²Geophysical Institute, University of Bergen, Bergen, Norway

³Finnish Meteorological Institute, Helsinki, Finland

⁴Institute for Atmospheric and Earth System Research, University of Helsinki, Helsinki, Finland

Correspondence

S. Wickström, Department of Arctic Geophysics, The University Centre in Svalbard PO Box 156, NO-9171 Longyearbyen, Norway.
Email: siiri.wickstrom@unis.no

Funding information

Academy of Finland, 317999

Abstract

We report an increase in winter (DJF) cyclone densities in the areas around Svalbard and in northwestern Barents Sea and a decrease in cyclone densities in southeastern Barents Sea during 1979–2016. Despite high interannual variability, the trends are significant at the 90% confidence level. The changes appear as a result of a shift into a more meridional winter storm track in the high-latitude North Atlantic, associated with a positive trend in the Scandinavian Pattern. A significant decrease in the Brunt–Väisälä frequency east of Svalbard and a significant increase in the Eady Growth Rate north of Svalbard indicate increased baroclinicity, favouring enhanced cyclone activity in these regions. For the first time, we apply composite analysis to explicitly address regional consequences of these wintertime changes in the high-latitude North Atlantic. We find a tendency toward a warmer and more moist atmospheric state in the Barents Sea and over Svalbard with increased cyclone activity around Svalbard.

KEYWORDS

Arctic, Barents Sea, Eady growth rate, extratropical cyclones, Scandinavian pattern, sea ice decline, storm tracks, Svalbard

1 | INTRODUCTION

Extratropical low-pressure systems (hereafter “cyclones”) are essential for the energetics of the atmosphere through transporting heat and moisture poleward, which is vital for balancing the net radiative cooling and fresh water deficit in the polar regions (Bengtsson *et al.*, 2006; Sorteberg and Walsh, 2008). Other impacts of cyclones on weather and climate in the Arctic are associated with high winds and precipitation. From an Arctic-wide perspective the cyclone density is highest in the summer (June–August, JJA) (Serreze and Barrett, 2008). However, the cyclone

activity, encompassing both the intensity and density of cyclones, in the high-latitude North Atlantic is highest in the winter (December–February, DJF) (Serreze *et al.*, 1993; Zhang *et al.*, 2004) with the highest density found at the northern periphery of the North Atlantic cyclone track; between mainland Norway and Svalbard and further to the east in the Barents and Kara Seas (Simmonds *et al.*, 2008).

The Arctic climate system is transferring into a warmer and wetter state as a result of the unequivocally warming climate (Intergovernmental Panel on Climate Change, 2013; Vihma *et al.*, 2016). The Arctic is warming fastest

in the autumn and winter seasons (Cohen *et al.*, 2014), and the highest warming rates are found around Svalbard and over the Barents Sea (Isaksen *et al.*, 2016; Kohne-
mann *et al.*, 2017). These areas have, in addition to rapidly rising air temperatures, experienced the highest rates of wintertime sea ice loss (Smetsrud *et al.*, 2010; Onarheim *et al.*, 2015; Onarheim and Årthun, 2017; Lind *et al.*, 2018) in the last few decades. On a more local scale, a decline in sea ice concentration related to increased rates of warm Atlantic water inflow has been observed in the fjords of western Spitsbergen (Cottier *et al.*, 2007; Muckenhuber *et al.*, 2016; Nilsen *et al.*, 2016). Several of the observed changes, both Arctic-wide and locally in Svalbard, have been hypothesized to be associated with climate change-driven large-scale atmospheric circulation changes in this region (Cottier *et al.*, 2007; Nilsen *et al.*, 2008; Isaksen *et al.*, 2016).

Large-scale pressure gradients and related properties (such as latitude, speed and meandering) of the polar-front jet stream drive the position and intensity of the extratropical cyclone tracks transporting heat and moisture poleward (Nakamura *et al.*, 2013; Cohen *et al.*, 2014). Compared to its Pacific counterpart, the North Atlantic storm track typically extends farther into the Arctic, thus making the Atlantic sector the primary gateway of atmospheric heat and moisture into the central Arctic (Tsukernik *et al.*, 2007; Sorteberg and Walsh, 2008; Naakka *et al.*, 2019). In addition to atmospheric heat transport, the oceanic heat mainly enters the central Arctic through the Barents Sea or through the Fram Strait (Aagaard and Greisman, 1975), making this area a hotspot for ocean–atmosphere energy exchange processes. The strength and orientation of the storm track reflect the large-scale state of the atmosphere. The question how large-scale atmospheric flow patterns have and will change in a rapidly warming climate has drawn a lot of attention in recent years (Screen *et al.*, 2018 and references within). Further, as Shepherd (2014) writes, “we have much less confidence in the atmospheric circulation aspects of climate change [compared to the thermodynamic aspect], which are primarily controlled by dynamics and exert a strong control on regional climate”. Regarding cyclones being an important component of atmospheric dynamics, several studies have addressed the question of how cyclone activity has changed and will change in the future Arctic (Rinke *et al.*, 2017; Zhang *et al.*, 2004; Sepp and Jaagus, 2011; Li *et al.*, 2014; Koyama *et al.*, 2017; Zahn *et al.*, 2018).

Positive trends in wintertime (DJF) cyclone density in the High Arctic are reported by several studies. Both Rudeva and Simmonds (2015) addressing the period 1979–2013, and Zahn *et al.* (2018) addressing the period 1981–2010, found statistically significant increases (at the 90% level, hereafter “significant”) in the cyclone frequency

north of the Canadian Arctic, over the Arctic Ocean and around Svalbard during these respective periods. Furthermore, they found a significant decrease in the cyclone frequency over the southern Barents Sea in the winter season. Rudeva and Simmonds (2015) used the ERA-Interim reanalysis (hereafter ERAI), from the European Centre for Medium-range Weather Forecasts (ECMWF) (Dee *et al.*, 2011) for quantifying these trends. Zahn *et al.* (2018) based their results on four different reanalyses, including the Climate Forecast System Reanalysis (CFSR: Saha *et al.*, 2006) from the National Centers for Environmental Prediction (NCEP), the Japanese 55-year reanalysis (JRA-55: Ebita *et al.*, 2011; Kobayashi *et al.*, 2015) from the Japan Meteorological Agency (JMA), and the Modern Era Retrospective analysis for Research and Applications version 2 (MERRA-2) reanalysis (Gelaro *et al.*, 2017), and ERAI. Zahn *et al.* (2018) report that the different reanalysis products are in good agreement in catching the overall atmospheric circulation patterns, differing, however, to some degree in the magnitude of the trends on a regional level. These differences probably result from the combined effects of differences in model resolution and model physics. Sepp and Jaagus (2011) analysed storm tracks derived from the NCEP/National Center for Atmospheric Research (NCAR) reanalysis dataset from 1948 to 2002, and found a significant increase in the number of cyclones entering the central Arctic. This result was, however, not driven by an increase in the number of cyclones entering from the North Atlantic, but rather from the Pacific sector of the Arctic. However, we note that the NCEP/NCAR reanalysis is the coarsest of the mentioned reanalysis products, with a $2.5^{\circ} \times 2.5^{\circ}$ horizontal resolution, and is hence likely less reliable on a regional scale.

The majority of the studies on Arctic cyclones have had primarily the circumpolar perspective with little regional focus. In this study, we focus on the regional changes in cyclone activity in the high-latitude North Atlantic, identified and recognized to be important for both atmospheric and oceanic poleward heat transport as well as climate change, as outlined above. The objectives of this study are (a) to quantify the cyclone climatology and trends (1979–2016) in the high-latitude North Atlantic, (b) to better understand the regional consequences of these trends, and (c) to ascertain the mechanisms possibly responsible for the cyclone climatology changes.

This article is structured as follows: in Section 2 we briefly describe the data, the cyclone tracking algorithm and analysis methods used in this study. Thereafter, in Section 3, we aim to answer the main objectives by presenting and discussing (a) seasonal climatology and trends of cyclone density and cyclone activity within the high-latitude North Atlantic, (b) composite analysis of key climate variables for areas showing significant trends in

winter cyclone density, and (c) trends in climate indices and baroclinicity. In Section 4 we discuss the results in the context of previous studies and conclude the study.

2 | MATERIALS AND METHODS

2.1 | Cyclone tracking

There are a number of different methods for defining and tracking cyclones (Murray and Simmonds, 1991; Hodges, 1995; Serreze, 1995). In our study we utilize the Melbourne University cyclone tracking scheme (Murray and Simmonds, 1991), which is shown to perform well in a number of comparison studies (Neu *et al.*, 2013; Simmonds and Rudeva, 2014). This cyclone tracking scheme builds upon scanning a given mean sea-level pressure (MSLP) field and comparing the Laplacian of the pressure field between adjacent grid points. After identifying a pressure depression, an iterative approximation to the centre of the ellipsoid of best fit to the MSLP field is used to locate the low-pressure centre. A physical interpretation of the Laplacian of the pressure field is that it can be seen as a measure of the cyclone intensity (Petterssen, 1956). In the Melbourne University tracking scheme, the threshold for the average value of the Laplacian is set to $0.2 \text{ hPa}\cdot(^{\circ} \text{ latitude})^{-2}$ by default over a radius of 2° for depressions to be recognized as cyclones. In this study, however, we focus only on strong cyclones that have an average value of the Laplacian above $0.7 \text{ hPa}\cdot(^{\circ} \text{ latitude})^{-2}$ with a defined centre (closed). Also, to avoid erroneous results due to extrapolation of MSLP over regions with high orography, we neglect data from the regions above 1,000 m above sea level (ASL) that is, mainly Greenland in our domain of interest. We also filter out cyclones with lifetimes shorter than 48 h (8 track points). In this work we track explicitly extratropical cyclones in the high latitudes and these should not be confused with polar lows.

Several studies have proved the high quality of ERAI (Dee *et al.*, 2011) in the Arctic (Dufour *et al.*, 2016; Koyama *et al.*, 2017; Naakka *et al.*, 2018), and we therefore chose to use the MSLP fields from ERAI (at the native horizontal grid resolution of $0.75^{\circ} \times 0.75^{\circ}$) for the cyclone tracking. We ran the cyclone tracking algorithm for the time period from 1979 to 2016, with a 6 h output interval.

2.2 | Analysis of track data

For the cyclone track statistics, we binned the cyclone track points geographically in boxes of $400 \text{ km} \times 400 \text{ km}$ (indicated in the map in Figure 2a). Given the typical horizontal length and velocity scales of synoptic-scale

cyclones, we found this bin size to be appropriate without compromising on the horizontal resolution.

We refer to the number of cyclone track points per season within each of the geographical bins as the “cyclone density”. Furthermore, following Zhang *et al.* (2004) we use a cyclone activity index (CAI) to integrate information on cyclone intensity, frequency, and duration in each geographical bin. For a given season and geographical bin, this index is defined as the cyclone density times the mean cyclone intensity;

$$CAI = \text{cyclone density} \times \text{cyclone intensity}, \quad (1)$$

where the intensity is defined as the Laplacian of the pressure field (Petterssen, 1957). The mean cyclone intensity refers to the mean of the intensities of the cyclones in a given box at a given time.

We used the non-parametric Theil–Sen slope estimator (Theil, 1949; Sen, 1968; Eqn (9) in Yilmaz and Perera, 2015) for calculating the magnitude of the linear trends in both cyclone density and cyclone activity.

2.3 | Statistical significance

In order to quantify the statistical significance of the temporal trends in cyclone density, we have used the well-established Mann–Kendall type *t*-test (Mann, 1945; Kendall, 1975). The Mann–Kendall test is a non-parametric test, which means that no assumption is made about the sample size nor about a normal distribution. Also, being a rank-based test the Mann–Kendall test is less sensitive to outliers, relative to parametric tests. The exact equations used in our work can be found as Eqns (1)–(4) in Yilmaz and Perera (2015).

Furthermore, we used Monte-Carlo simulations to assess the significance of anomalies between the climatology and composites of the different climate variables. These simulations are done by picking out random time series, with the same length as the composite, from the seasonal climatology. In our study this procedure was repeated 1,000 times to produce a synthetic probability distribution. The original composite is considered statistically significant if it is at the 90th percentile of this probability distribution. As it turns out, the mentioned anomalies are statistically significant virtually everywhere and we therefore decided not to indicate this significance in the presentation of the corresponding results in Section 3.

2.4 | Composite analysis

To gain an understanding of the regional impacts of cyclone activity, we calculate composites for the nine key climate variables: MSLP, 2 m air temperature, turbulent

fluxes (latent + sensible heat fluxes), long-wave radiation (decomposed into upwelling and downwelling), Z500 – Z1000 geopotential layer thickness, precipitation and vertically integrated divergence of dry static (“thermal” in ERAI) and latent-heat energy fluxes. The latter energy flux is derived from the corresponding moisture flux field in ERAI.

The composites of each field are defined as the mean of the field (daily resolution) for cases with cyclone activity in the regions of interest (defined in Figure 1). The difference between the seasonal mean field of these variables and the composites is the anomaly.

2.5 | Eady growth rate

We calculate the 500 hPa Eady growth rate (Eady, 1949), as is done by for example, Koyama *et al.* (2017):

$$EGR = 0.31 * \frac{f}{N} \frac{dv}{dz}. \quad (2)$$

Here f is the Coriolis parameter, N is the Brunt–Väisälä frequency, dv/dz is the vertical wind shear, \mathbf{v} is the horizontal wind vector and z is the height of the atmospheric layer of interest. Following Simmonds and Lim (2009) and Koyama *et al.* (2017) we use the atmospheric layer encompassed by the 300 and 700 hPa pressure levels. The vertical wind shear dv/dz is related to the horizontal temperature gradient via the thermal wind equation (Wallace and Hobbs, 2006). The Brunt–Väisälä frequency is a measure of atmospheric static stability given by:

$$N = \sqrt{\frac{g}{\theta} \frac{d\theta}{dz}}. \quad (3)$$

Here g is the gravitational acceleration, θ is the potential temperature, and $d\theta/dz$ is the vertical gradient of potential temperature. We use the 300, 500 and 700 hPa pressure-level potential temperatures in calculating N at each grid point. Hence, the Eady growth rate depends on both the static stability and horizontal temperature gradients in the atmosphere.

The zonal and meridional winds, air temperature, and geopotential height fields are taken directly from the ERAI reanalysis and the potential temperature field is calculated utilizing the temperature and pressure fields from ERAI. As recommended by Lim and Simmonds (2009), daily averages are used for the Eady growth rate calculations.

3 | RESULTS

3.1 | Seasonal changes in cyclone activity

Figure 1 presents a map of our study region, encompassing the area 60°W to 70°E and 64°N to 90°N. The region

was chosen to capture extratropical cyclone activity over the North Atlantic and all the way to the Central Arctic, through the Fram Strait and via the Barents Sea.

In the high-latitude North Atlantic, we observe the highest cyclone densities in the Fram Strait and southern Barents Sea in all seasons except summer (Figure 2a,e,i,m). The average seasonal cyclone density in these regions is up to 16 cyclone track points in a 400 × 400 km domain during a 3-month season, translating to over five cyclone track points per month. This is a result of the North Atlantic storm track splitting in two distinct branches as it approaches Svalbard from the southwest. Especially in the winter (DJF) and autumn (September–November, SON) seasons a high cyclone density band reaching from Iceland into the Arctic is evident (Figure 2; location names in Figure 1), than in the Fram Strait and Barents Seas (Figure 2i). This is in agreement with Serreze and Barret (2008), who also found high cyclone densities in the summer for the Central Arctic. However, whereas they found these to be the highest cyclone densities for any season and region, we find the highest densities in the Central Arctic in SON. However, we note that our study region only covers the parts of the Central Arctic located within 60°W and 70°E.

As expected, the seasonal geographical patterns in CAI (Figure 2c,g,k,o) follow closely the geographical patterns in cyclone density (Figure 2a,e,i,m), however, with some differences between the seasons. The cyclone densities in the Barents Sea and the Fram Strait are rather similar in SON, DJF and March–May (MAM), while DJF generally has the highest CAI for these areas. This is because the DJF cyclones are on average more intense than the MAM and SON cyclones. This agrees well with several previous studies documenting the North Atlantic storm track activity being highest in the winter (Zhang *et al.*, 2004). Furthermore, we see that the difference between the JJA CAI and the CAI in the rest of the seasons is even more pronounced than the differences between the seasonal cyclone density fields. This indicates that the cyclones, in addition to being fewer in summer in the Fram Strait and the Barents Sea, are also weaker (have lower intensity) compared to the other seasons.

Considering trends in cyclone densities over the period 1979 to 2016, we see the strongest ones in DJF (Figure 2b), which is in line with previous studies (Rudeva and Simmonds, 2015; Zahn *et al.*, 2018). In the Fram Strait, Greenland Sea and Barents Sea regions, we find the strongest positive trends around Svalbard. These are +1.3 cyclone track points per decade west of Svalbard (hereafter Region A) and +3 cyclone track points east of Svalbard (hereafter Region B). The strongest negative trends of –4.5 cyclone track points per decade are located in the southern Barents Sea (hereafter Region C). The Regions A, B and C are

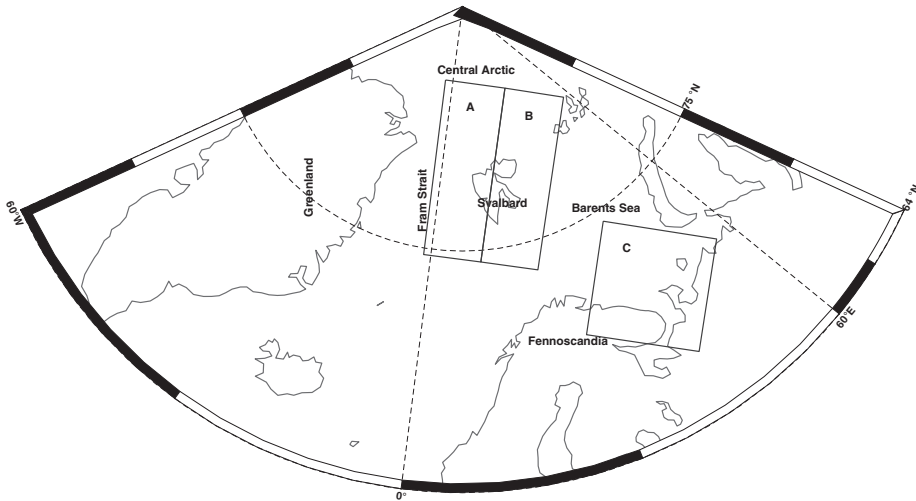


FIGURE 1 Map showing the domain of interest in this study and labels on relevant oceans and air masses

marked in Figure 1, along with the names of geographic regions. The positive trends in cyclone density are significant in all individual patches in Region B and in half of the patches in Region C (Figure 2b).

Considering temporal variability in DJF cyclone densities across the regions A, B and C on an annual level (Figure 3), we see that Regions A and C have average annual densities in the range between 5 and 25 cyclone track points (Figure 3a,c), with the total cyclone track point count for the whole period being 1,487 and 1,950 respectively. The corresponding range for Region B is from 1 to 22 cyclone track points, with a total of 1,194 track points (Figure 3b). The generally lower cyclone densities in region B compared to Regions A and C can be explained by the climatological positions of the DJF North Atlantic storm track branches over the Fram Strait and the southern Barents Sea (Figure 3a). All regions show a large inter-annual variability as expected with the turbulent nature of extratropical cyclones. Furthermore, we see that all of these regions have significant trends at the 90% confidence level when all parts of the regions are considered (Region A: $p = .082$, Region B: $p = .08$ and Region C: $p = .009$).

Returning to trends in cyclone densities for the other seasons, spatially almost similar, but generally weaker trends in cyclone density, compared to DJF, are found in SON (Figure 2n). MAM trends (Figure 2f) are similar to those in winter in the western Barents Sea and east of Svalbard (around Region B), but opposite in the Fram Strait (Region A, a weak decrease in cyclone density) and in the southern Barents Sea (Region C, insignificant increase). The JJA trends are rather different from the other seasons;

there is a significant negative trend in cyclone density northwest of Svalbard (northern parts of Region A) and a significant positive trend just east of Region B and in parts of Region C (Figure 2j).

CAI (Figure 2d,h,p) shows similar spatial patterns to the trends in cyclone density for all four seasons, but fewer geographic bins have statistically significant values. The difference between significance in the trend fields of cyclone density and CAI coincides with cyclone intensity trends (not shown) being insignificant for this period.

As described above, the strongest trends in both cyclone density and CAI, in the high-latitude North Atlantic, are found in DJF. In addition, together with SON, DJF is the season where the strongest near-surface warming rates are found (Cohen *et al.*, 2014). Hence, to limit the scope of this study, we hereafter only focus on the DJF season.

3.2 | Composite analysis

A central aim of this study is to better understand the regional-scale consequences of changes in DJF cyclone activity. To this end, we have calculated the difference between the seasonal mean and the composite of events with a cyclone centre in each region (Regions A, B and C) to produce anomalies for the following fields: MSLP, 2 m air temperature, turbulent fluxes, long-wave radiation, Z500 – Z1000 layer thickness, precipitation and vertically integrated divergence of latent and dry static energy fluxes, as described in Section 2.3. The number of cases used in

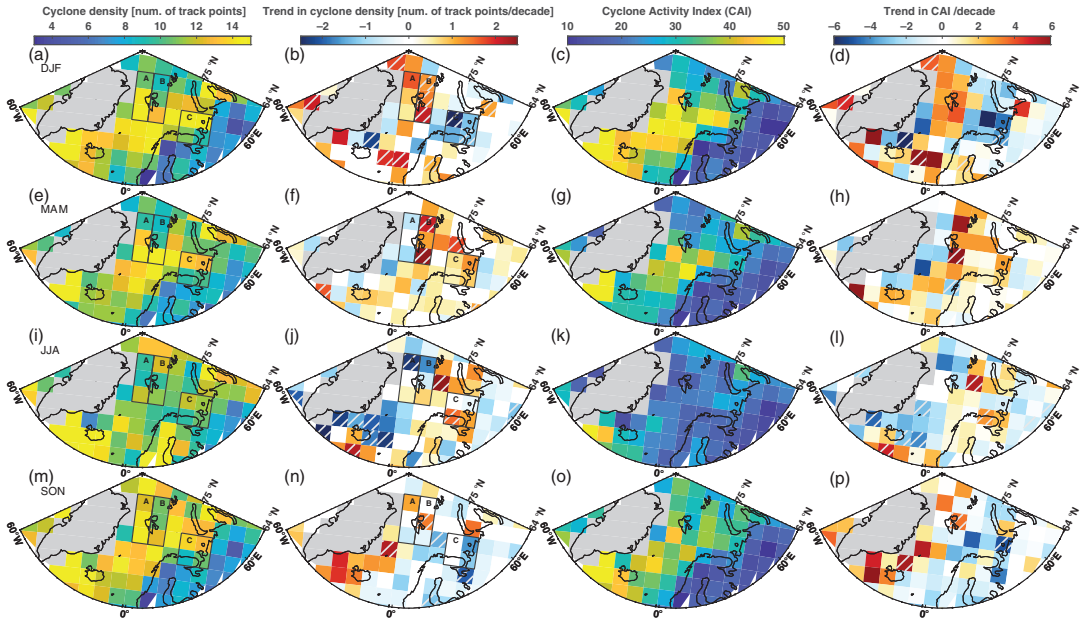


FIGURE 2 (a–p) Seasonal (rows) climatology and trends of cyclone density (number of track points in a given grid box per season) (columns 1 and 2) and cyclone activity index (CAI) (columns 3 and 4) for the period 1979–2016. The grid shows the 400×400 km geographical bins used for the cyclone track data. The hatching marks the bins with a significant trend (90% level). Greenland is filtered out due to high elevations. The boxes labelled A, B and C are the areas we have identified as hot spots of DJF change in cyclone density

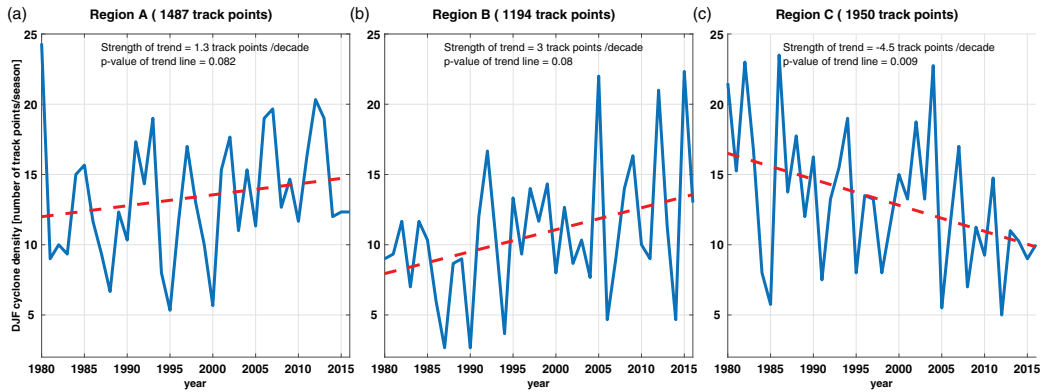


FIGURE 3 Time series of DJF cyclone density and the linear trend in the period 1979–2016 in (a) the Fram Strait (region A), (b) East Svalbard (region B) and (c) the southern Barents Sea (region C). The title indicates how many DJF cyclone track points were located in these regions during the study period

calculating the anomalies for each region is indicated in Figure 3.

The climatological mean fields of MSLP, 2 m air temperature, and daily precipitation are shown in Figure 4a–c respectively. MSLP anomalies of events with a cyclone in

Region A (Figure 4d), west of Svalbard, show 5 hPa lower than climatology MSLP values in the Fram Strait and up to 8 hPa higher pressure over most of Fennoscandia. The 2 m air temperatures are slightly above their climatological values (1–2 K) along the North Atlantic storm track. As would

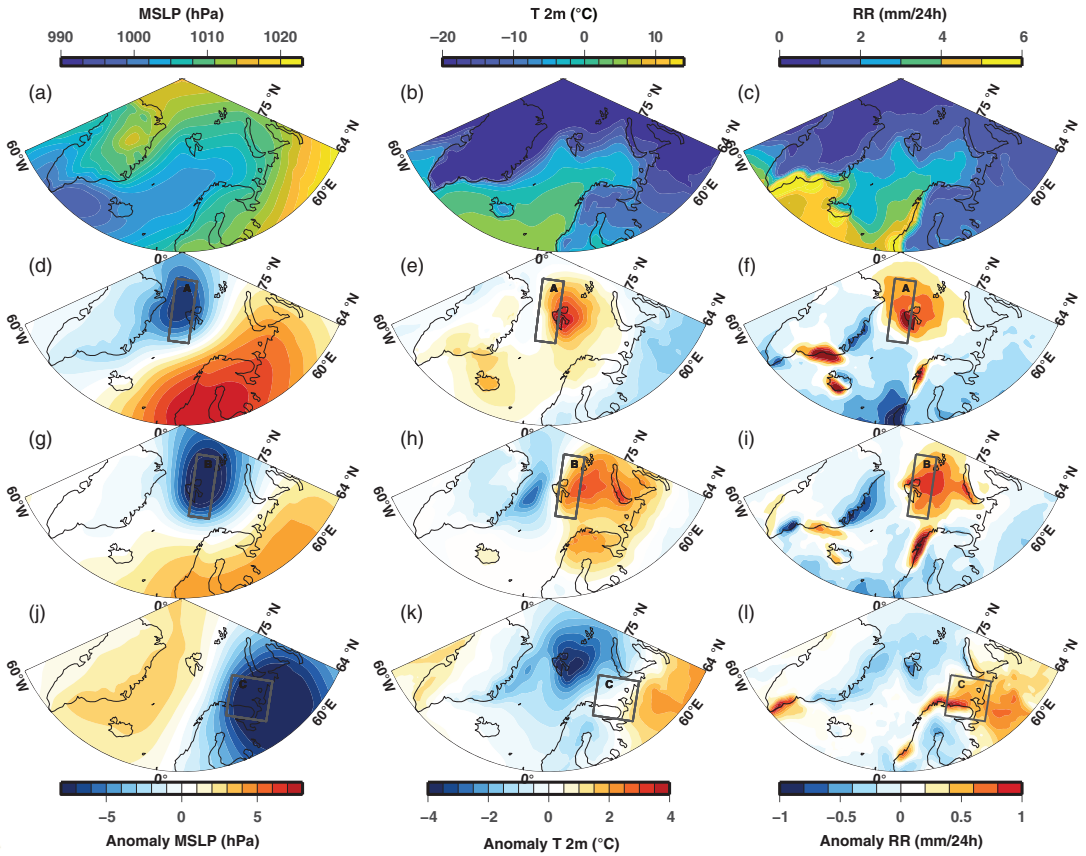


FIGURE 4 DJF climatology of (a) mean sea-level pressure (MSLP), (b) 2 m air temperature (T), (c) precipitation (RR), and composites from these when a cyclone centre is in (d–f) region A, (g–i) region B and (j–l) region C. The sign convention is such that all fluxes are defined positive (negative) toward (away from) the surface

be expected in a warm sector of an extratropical cyclone, the strongest positive anomaly (up to 4 K) is located over Svalbard and extends to the north and east (Figure 4e). These events are also associated with a positive precipitation anomaly, which has the highest values (up to 1 mm per 24 h) for about the same region as the strongest positive temperature anomaly (Figure 4f). The alignment of the strongest positive precipitation and temperature anomalies agree well with the warm sector and the associated frontal precipitation in an extratropical cyclone.

Compared to MSLP anomalies for Region A, the anomalies for Region B are shifted eastward with the lowest surface pressure in the western Barents Sea (Figure 4g). Also, the negative MSLP anomaly for Region B is stronger (–8 hPa), and the positive anomaly over Fennoscandia and northwestern Russia is weaker (4 hPa). The difference in the negative MSLP anomalies between composites for Regions A and B is probably a consequence of Region

A being closer to the Fram Strait branch of the North Atlantic storm track than Region B. In line with the pressure anomaly, the 2 m air temperature anomalies are also shifted eastward, with anomalously warm (up to 4 K above climatology) temperatures over most of the Barents Sea and northern Scandinavia and cold (down to –2 K below climatology) over the Fram Strait (Figure 4), when compared to composites for Region A. The cyclonic flow, deduced from the pressure (anomaly) patterns, centred on Region B sets up a flow pattern with warm-air advection over the Barents Sea and cold-air advection over the Fram Strait. As expected in a warm sector of an extratropical cyclone (Bjerknes, 1919), a positive precipitation anomaly of up 1 mm per day aligns well with the warm temperature anomaly over the Barents Sea (Figure 4i).

During the events with a cyclone in Region C (southern Barents Sea), the MSLP field is characterized by a positive anomaly of up to 3 hPa along the east coast of

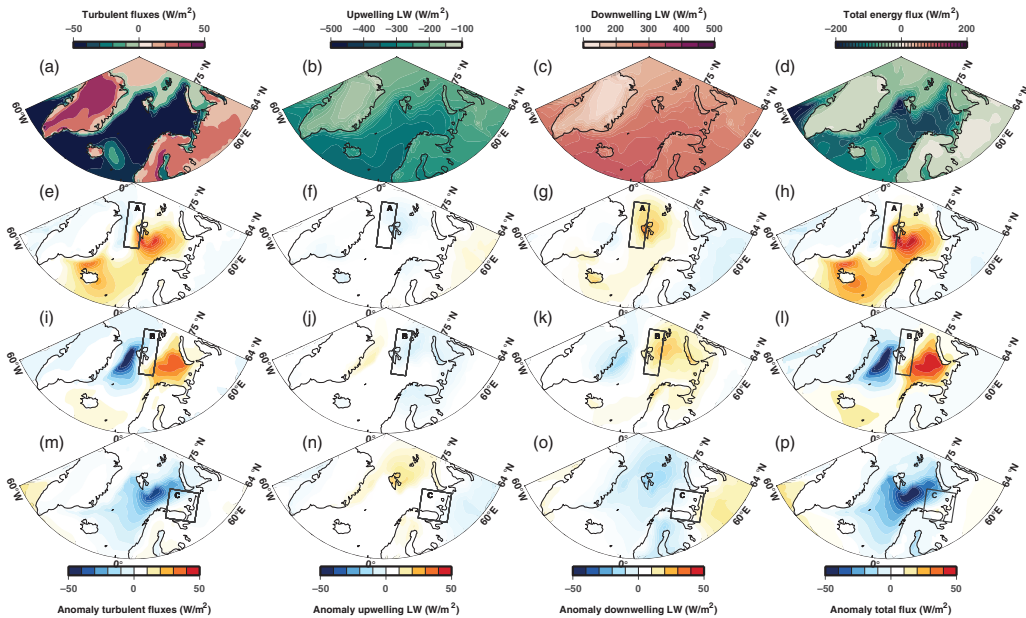


FIGURE 5 Four DJF climatologies of (a) turbulent fluxes (latent and sensible), (b) surface to atmosphere long-wave (thermal) radiation (defined negative), (c) atmosphere to surface long-wave (thermal) radiation (defined positive), (d) total flux (sum of (a), (b) and (c)), and composites from these when a cyclone centre is in (e–h) region A, (i–l) region B and (m–p) region C. The sign convention is such that all fluxes are defined positive (negative) toward (away from) the surface

Greenland, setting up a northerly flow through the Fram Strait together with the negative anomaly over the southern Barents Sea reaching into northwestern Russia and Fennoscandia (Figure 4j). The resulting cold-air advection over Svalbard is accompanied by a negative 2 m air temperature anomaly, reaching -4 K in region B (Figure 4k). These events are also associated with a positive precipitation anomaly of up to 1 mm per 24 h over the northern coast of Fennoscandia and southeastern Barents Sea, leaving the rest of the high-latitude North Atlantic drier than the climatology (Figure 4l). This precipitation anomaly again follows the temperature anomaly. However, the intensification of the anomaly at the coast is most likely orographic enhancement of precipitation.

Anomalies of surface fluxes of turbulent heat and long-wave radiation are a key for understanding the regional consequences of changes in DJF cyclone density on the surface energy balance. We define the fluxes from the point of view of the surface, where positive (negative) fluxes are directed toward (away from) the surface. The high-latitude North Atlantic experiences polar night most of DJF and, hence, solar short-wave radiation is neglected in this study.

The climatological sea ice extent is seen in the DJF climatological turbulent energy flux fields (Figure 5a), with

generally a turbulent energy gain over land masses and sea ice and a loss over the open sea. A transition zone of slightly negative turbulent fluxes (-10 to 0 $W\cdot m^{-2}$) between the open water and the positive fluxes in the Central Arctic marks the marginal ice zone. In these regions, the DJF thermal long-wave radiative balance contributes to the net surface cooling, with the seasonal average of the upwelling component (Figure 5b) dominating over the downwelling component (Figure 5c).

The events with a cyclone centre in Region A are associated with a positive turbulent flux anomaly (less heat loss) up to 40 $W\cdot m^{-2}$ covering the southwestern parts of the Barents Sea and reaching to the west coast of Svalbard (Figure 5d). Given the climatological turbulent heat loss of similar magnitudes in these regions (Figure 5a), the net turbulent flux approaches zero or the sign of the flux reverses, turning the atmosphere into a weak turbulent heat source during these events. In the western Fram Strait there is a weak negative (stronger surface heat loss) turbulent flux anomaly down to -10 $W\cdot m^{-2}$, corresponding to a cold-air outbreak regime in that region, set up by the northerly wind field advecting cold and dry Arctic air masses over relatively warm open water.

The composites for the events with a cyclone centre in Region A show an increase in both the upwelling

(the negative anomaly in Figure 5e) and downwelling long-wave radiation (positive anomaly in Figure 5f) around Svalbard. The downwelling radiation anomaly is positive in a band from Iceland into the Barents Sea, indicating an active North Atlantic storm track with associated frontal clouds. A thick frontal cloud, typically associated with extratropical cyclones, is one of the most efficient processes in raising surface temperatures in the Arctic in the dark season (Vihma and Pirazzini, 2005). The upwelling long-wave radiation has a negative anomaly above Svalbard reaching into the Central Arctic and the northern Barents Sea. No strong anomaly is seen to the southwest, contrary to the downwelling radiation. There is a geographic mismatch between anomalies in upwelling and downwelling long-wave radiative components (Figure 5e,f) over the open ocean. Even though the upper ocean receives more heat when cyclones are in Region A, its impact on the surface temperature and, hence, on upwelling long-wave radiation remains minor because the heat received via downwelling long-wave radiation is mixed in the ocean surface layer with a large heat capacity.

With a cyclone in region B, a positive anomaly of $40 \text{ W}\cdot\text{m}^{-2}$ covers most of southeastern Barents Sea and a corresponding negative anomaly of $-40 \text{ W}\cdot\text{m}^{-2}$ is centred on the Fram Strait. These anomalies are well in agreement with the northerly wind field set up on the western side of the cyclone centre located in Region B, advecting cold air masses from the Central Arctic over the relatively warm ocean in the Fram Strait and the south-southwesterly flow bringing warm air over the Barents Sea on the eastern side of the cyclone. The upwelling long-wave radiative flux is a function of the surface temperature and, thus, the region in the northern Barents Sea with the strongest positive 2 m air temperature anomaly also has a negative outgoing long-wave radiative flux anomaly (more surface heat loss, Figure 5h). However, the anomalously high downwelling long-wave radiative flux driven by increased cloudiness in the warmer and more moist air masses exceeds that of the upwelling anomaly so that the anomaly of net long-wave radiation anomaly heats the surface (about $20 \text{ W}\cdot\text{m}^{-2}$) in Region B. The long-wave radiative anomalies have opposite signs in the western Fram Strait. Cold air advection and possible sea ice export in the East Greenland Current might account for the positive outgoing long-wave radiative anomaly (less than climatology surface heat loss), matching with a cold surface anomaly (Figure 4h).

The cold-air outbreak in the Fram Strait, driven by the flow field associated with a cyclone in Region B, with strong turbulent surface heat loss (Figure 5g), drives atmospheric convection. A positive anomaly in upwelling long-wave radiation (i.e. less long-wave radiation emitted by the surface) is present in the ice-covered western Fram Strait (Figure 5h), where the snow/ice surface temperature

rapidly responds to cold air. On the contrary, no anomaly is present in the open parts of the Fram Strait, because the sea-surface temperature is not sensitive to a synoptic-scale cold-air outbreak.

Cyclone activity in Region C, in contrast to Regions A and B, is characterized by large turbulent surface heat loss that is up to $40 \text{ W}\cdot\text{m}^{-2}$ stronger than the climatology southeast of Svalbard. In line with Figure 4b,k, the upward long-wave radiation has a positive anomaly over sea ice (Figure 5k) as the surface is losing less heat in these conditions due to the colder surface temperatures. Similarly, the downward long-wave radiation is anomalously low both in the Fram Strait and the Barents Sea in line with the relatively cold and dry air masses.

Finally, we consider the total energy flux (Figure 5d,h,l,p), which we have calculated as the sum of the turbulent and long-wave radiation energy fluxes. We see from the average of the entire time period (Figure 5d) that in sum the fluxes considered contribute generally to a net heat loss at the surface in the study area during DJF. Furthermore, it is clear that the turbulent surface energy fluxes dominate over the long-wave energy fluxes in forming the total energy flux anomalies connected to cyclones in Regions A, B and C (Figure 5h,l,p). Also, we note that the areas most strongly affected by these anomalies are the Barents Sea with surroundings waters and large parts of the Fram Strait.

Moving up from the surface layer; to gain an understanding of regional consequences in the free atmosphere, driven by cyclonic activity, the final part of the composite analysis focuses on anomalies in the Z500 – Z1000 layer thickness and vertical integrals of heat transport divergence. The climatological distribution of the geopotential layer thickness (Z500-Z1000) is close to zonal with a southward gradient (Figure 6a). The layer thickness is an indirect measure of the air-mass temperature in the mid- to low troposphere. Hence, the zero line in the Z500-Z1000 anomalies can be interpreted as the mean position of the baroclinic zone, with the given cyclone centre location. For both Regions A and B (Figure 6d,g) the Z500-Z1000 anomaly fields display air masses warmer (thicker) than climatology air masses over Fennoscandia and the Barents Sea (positive Z500-Z1000 anomalies of up to 50 m) and colder than climatology over the Fram Strait, which is in line with the above-discussed northerly wind field west of the cyclone centre. The positive Z500-Z1000 anomaly with relatively warm air masses reaches further north into the northern Barents Sea with cyclones in Region A, compared to Region B. Region A has also a more meridionally oriented baroclinic zone between the positive and negative anomalies running over Svalbard (Figure 6d,g). Region B has the baroclinic zone more zonally south of Svalbard. In these events the air masses over Svalbard are

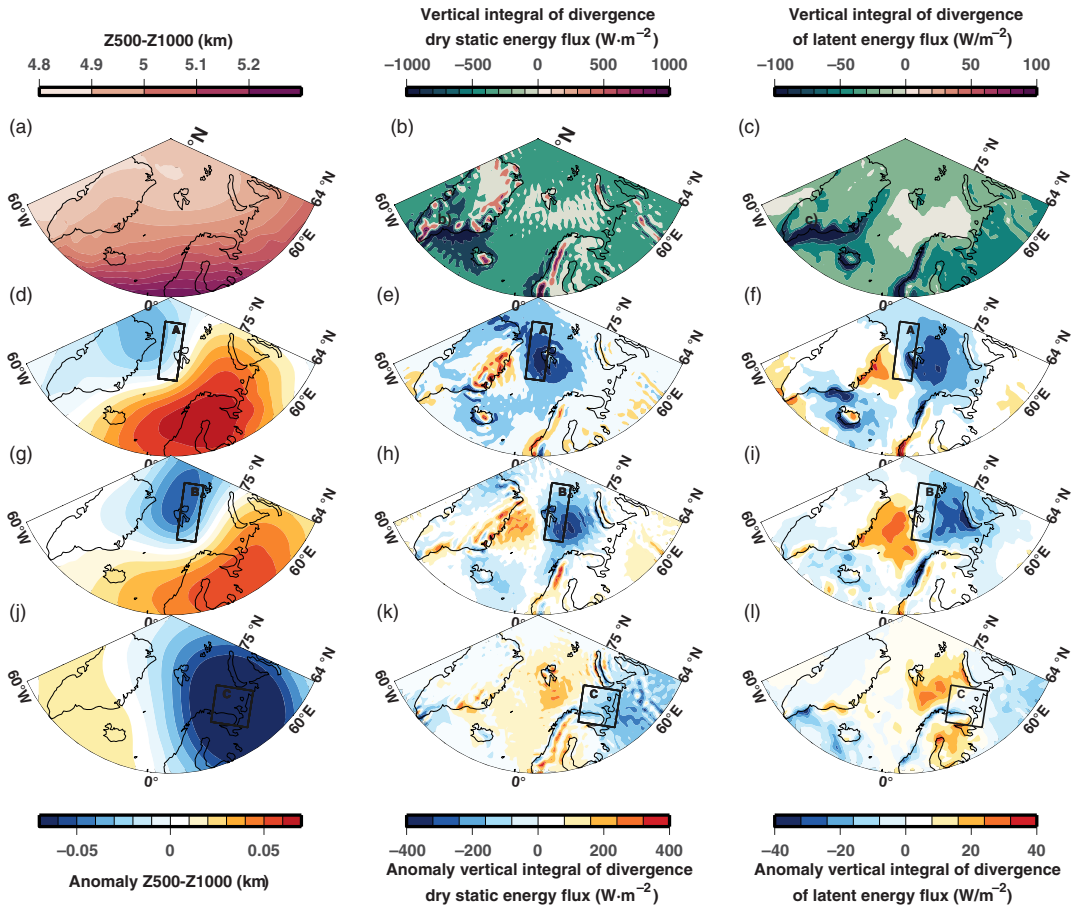


FIGURE 6 DJF climatology of (a) Z500 – Z1000, (b) vertical integral of divergence of dry static energy transport, (c) vertical integral of divergence of latent-heat transport, and the composites of their anomalies when a cyclone centre is in (d–f) region A, (g–i) region B and (j–l) region C

colder than the climatology. The negative anomaly, down to -50 m, for Region B (Figure 6g) is centred over the Fram Strait, being stronger than the corresponding anomaly for Region A (Figure 6d) with a -30 m anomaly centred over northeastern Greenland. The anomalies for Region C show a vast negative Z500-Z1000 thickness anomaly, down to -50 m, covering Svalbard, the Barents Sea, Fennoscandia and northwestern Russia (Figure 6j), suggesting that the air masses flowing around the cyclone centre are of Arctic origin.

To better understand the energetics related to the trends in cyclone activity, we here consider in the following anomalies of vertical divergence of the transport of latent heat and dry static energy over the full atmospheric column (Figure 6, columns 2 and 3). We note that the average DJF dry static energy transport convergence is an order of

magnitude larger than that of the latent heat (Figure 6b,c). In line with the net atmospheric poleward transport of energy, convergence dominates over the northern North Atlantic for both dry static energy and latent heat, the DJF mean being close to zero or slightly negative in Regions B and C (Figure 6c).

For cyclone centres in the Fram Strait (Region A), both the dry static energy and latent-heat transport divergence have negative anomalies over and around Svalbard (Figure 6e,f), indicating above-climatology heating in the region. The anomalies in the divergence in the dry static energy transport are larger than those of the latent heat. Region B has similar bimodality as Region A, with dry static energy and moisture transport convergence east of the Svalbard archipelago and divergence in the Fram Strait. This bimodal distribution aligns well with

TABLE 1 DJF trends in climate variables over the period 1979–2016 (change per decade)

	Region A	Region B	Region C
2 m air temperature (°C)	Trend: 1.1 °C/decade ($p < .001$)	Trend: 0.69 °C/decade ($p < .001$)	Trend: 0.58 °C/decade ($p < .001$)
Upwelling long-wave radiation ($W \cdot m^2$)	Trend: 3.9 $W \cdot m^2$ /decade ($p < .001$)	Trend: 2.6 $W \cdot m^2$ /decade ($p < .001$)	Trend: 2.1 $W \cdot m^2$ /decade ($p < .001$)
Downwelling long-wave radiation ($W \cdot m^2$)	Trend: 4.2 $W \cdot m^2$ /decade ($p < .001$)	Trend: 2.6 $W \cdot m^2$ /decade ($p < .001$)	Trend: 3.2 $W \cdot m^2$ /decade ($p < .001$)
Z500 – Z1000 layer thickness (km)	Trend: 0.01 km/decade ($p = .02$)	Trend: 0.01 km/decade ($p = .09$)	Trend: 0.01 km/decade ($p = .000$)

Note: The regions A, B and C are indicated on the map in Figure 2a.

the synoptic situation with cold-air advection west and warm-air advection east of the cyclone centre. In Region C, the divergence fields have a positive anomaly indicating larger-than-climatological cooling effect, in line with advection of cold and dry air over the region in cases with cyclones in Region C.

To summarize the local impacts of DJF cyclone activity: with cyclone activity in Regions A and B, the Greenland Sea and Barents Sea regions experience warmer and wetter winter conditions (Figure 4e,h,f,i), whereas with cyclone activity in Region C, the composites are colder and drier than the DJF climatology in regions A and B (Figure 4k). The MSLP field associated with composites of Regions A and B indicate a northerly wind in the Fram Strait, west of the cyclone centre, advecting cold air into Regions A and B with a compensating southerly wind to the east of the centre (Figure 4d,g). This is seen as an anomalous surface heat loss (gain) in the regions with cold (warm) advection in both the turbulent flux and long-wave radiative fields (Figure 5e–p). Region C is again showing generally colder and drier conditions over Svalbard, with a net surface heat loss in most of the Barents Sea (Figures 4k,l and 5p).

Further, we have calculated the trends in the climate variables (Table 1). At a 95% significance level we find a warming trend in all regions of interest (Region A: 1.1 °C/decade, Region B: 0.67 °C/decade and Region C: 0.58 °C/decade). Also, both upwelling and downwelling long-wave radiation have significant positive trends reflecting surface warming and increase in the cloudiness and water vapour in the atmosphere. In line with the general warming, the Z500–Z1000 layer thickness has a positive trend of 10 m/decade. The trend in the Z500–Z1000 layer thickness is, however, significant only in Region A. MSLP, precipitation intensity, turbulent fluxes and the vertically integrated divergent fluxes of dry static energy and latent heat do not have significant trends in the regions of interest.

3.3 | Trends in cyclone densities and their relation to climate indices

We have so far shown that the cyclone densities have significant temporal trends around Svalbard (Regions A and B) and in the southeastern Barents Sea (Region C), and our composite analysis suggests that the consequences of these changes are warmer and wetter winter conditions around Svalbard (Figures 4–6). We now move on to the third, and last objective of the study; connecting the documented cyclone density trends to larger-scale climate indices and, in Section 3.4, to baroclinicity.

The temporal and spatial variability in cyclone tracks is related to the variability in the surface pressure field, and, thus, to climate indices (typically derived from empirical orthogonal functions of the MSLP field) characterizing such variability. We here correlate three well-established climate indices encompassing the North Atlantic: the Scandinavian pattern (SCA), the Arctic Oscillation (AO) and the North Atlantic Oscillation (NAO) with the DJF cyclone densities. The indices were downloaded from the National Weather Service Climate Prediction Center (<https://www.cpc.ncep.noaa.gov/data>). Positive phases of AO and NAO indicate a zonal polar tropospheric jet stream (Barnston and Livezey, 1987). Opposite to AO and NAO, the positive phase of the SCA (Barnston and Livezey, 1987) represents a large-scale atmospheric state with a high-pressure ridge, typically a blocking high, over the Scandinavian peninsula. This pattern favours a meridional storm track, steering cyclones into the Fram Strait rather than into the southern Barents Sea and northern Scandinavia (Bueh and Nakamura, 2007; Vihma *et al.*, 2019).

The results from our correlation analysis (Figure 7) show that for SCA the correlations are predominantly negative in the region from Iceland to the Barents Sea and positive in the Fram Strait. Hence, the correlation pattern of SCA and cyclone density is roughly the opposite of that

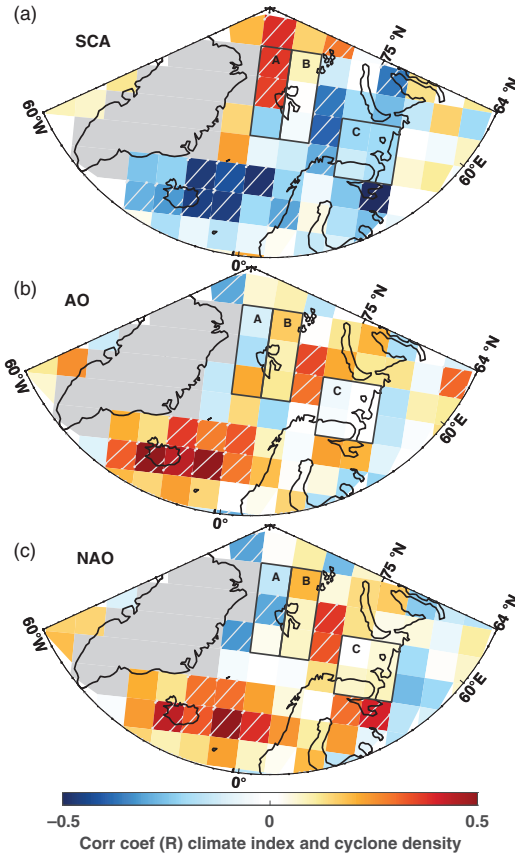


FIGURE 7 Correlation between DJF cyclone densities (number of track points) and (a) the Scandinavian pattern, (b) the Arctic Oscillation and (c) the North Atlantic Oscillation. The boxes labelled A, B and C are the areas we have identified as hot spots of DJF change in cyclone density. Areas where the trends are significant (90% level) are hatched

of AO and NAO (Figure 7b,c), which display negative correlations in larger parts of the Fram Strait and positive correlations around Iceland and the central Barents Sea. NAO can be considered a local (Atlantic) component of AO and it is not surprising that these indices have similar correlation patterns with cyclone density in the study region.

Amongst the climate indices, SCA generally displays the strongest correlations with the cyclone densities for Regions A, B and C. The trend in SCA over the time period of interest is positive (trend = 0.013/year, $p = .16$). Furthermore, there are significant positive correlations between SCA and cyclone density within Region A and significant negative correlations in the vicinity (west) of Region C.

Thus, the positive trend in SCA, though not statistically significant, supports to some degree the documented positive (Regions A and B) and negative (Region C) trends in cyclone densities.

3.4 | Changes in baroclinicity

Baroclinicity is a key driver for intensification and persistence of extratropical cyclones.

Central parameters in this regard are N and EGR , the latter of which is a measure of baroclinic instability at the mid-tropospheric level and, thus, a measure of the potential for cyclones to develop and grow (see Equation 2 in Section 2). N is the buoyancy frequency (see Equation 3 in Section 2), which is incorporated in EGR together with the vertical wind shear, accounting for the buoyant fraction of the available potential energy for cyclone intensification and persistence in the given layer. Both parameters have been applied several times in previous studies to assess changes in extratropical cyclones (Simmonds and Lim, 2009; Koyama *et al.*, 2017).

The DJF climatology of N (Figure 8a) shows, as expected, a positive meridional gradient (increasing with increasing latitude). At 64°N , N is around 0.0105 s^{-1} and at 90°N it is around 0.013 s^{-1} . We find a negative trend in the DJF N in the Greenland Sea and the Barents Sea regions in the period 1979–2016 (Figure 8c). This trend likely reflects the observed winter warming in these regions, which is strongest close to the surface (Cohen *et al.*, 2014). The negative trend in N is significant ($p < .1$, hatched areas in Figure 8c) in most parts of Region B and in one patch in Region C.

The DJF climatology of EGR (Figure 8b) shows a northward decreasing potential for cyclone growth, which is in agreement with the northward increasing static stability (Figure 6a), as EGR is an inverse function of N . In DJF, EGR has a significant positive trend north of Svalbard ($3 \times 10^{-3}\text{ day}^{-1}$) reaching to the North Pole (Figure 8d). This is a region with climatologically high static stability and low EGR in winter (Figure 8a,b). Further, in addition to N , EGR is a function of the mid-tropospheric wind shear, which is often dominated by the strength of the tropospheric jet stream. In the high-latitude North Atlantic region, the Arctic front jet stream is the most likely source of wind shear. Since the statistically significant changes in N mostly do not align with the statistically significant changes in EGR , we attribute the changes in EGR to changes in the wind shear rather than N . Consequently, this indicates an increased frequency of events with increased wind shear over Svalbard and north of it manifested as positive trends in EGR (Figure 8d).

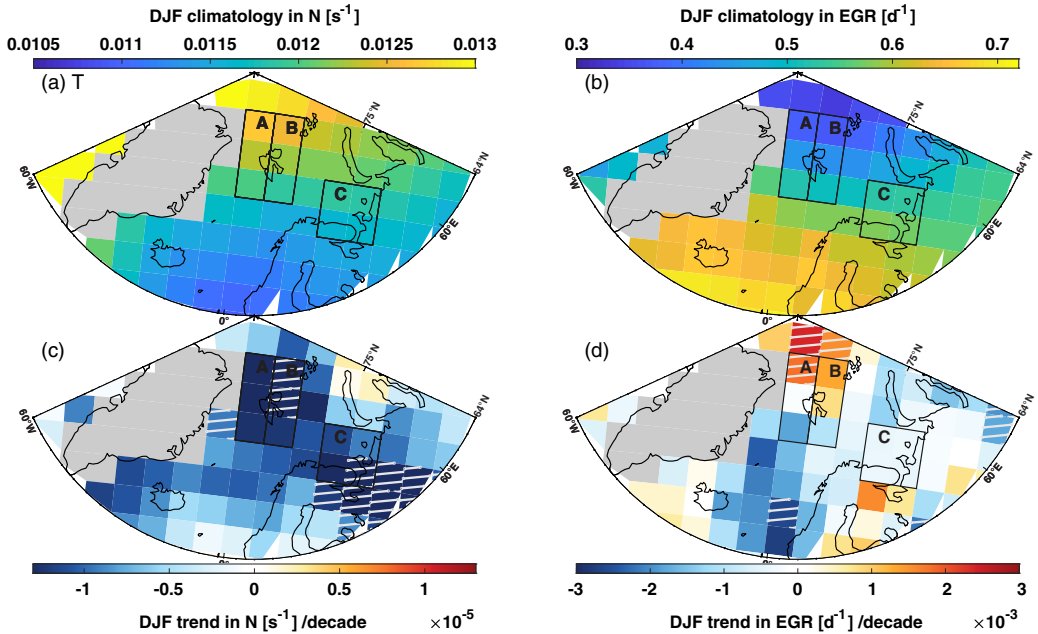


FIGURE 8 DJF climatologies of (a) static stability (N) and (b) Eady growth rate (EGR) and trends in (c) N and (d) EGR for the period 1979–2016 (see Section 2 for definitions of N and EGR). Areas where the trends are significant (90% level) are hatched. Greenland is filtered out due to high elevations

We find a positive trend in EGR over parts of and north of Svalbard and this is close to regions (Regions A and B) where we find significant positive trends in cyclone density. To the south of Svalbard, we find negative trends in EGR , but these are mostly insignificant.

Our results on baroclinicity show that there have been significant changes in both EGR and N in the vicinity of our regions of interest. These results suggest that atmospheric energetics in DJF has become more favourable for cyclone birth and development. The increased EGR and decreased N support cyclone trajectories penetrating further north, and hence, support the positive cyclone density trends found in Regions A and B.

Several previous studies have found a northward shift in the cyclone track within our study region (e.g. Tamarin-Brodsky and Kaspi, 2017). It is an intriguing question whether the observed increase in cyclone densities in Regions A and B, and the corresponding decrease in Region C, are parts of a local component of such a shift. The documented correlations between SCA and cyclone densities within these areas would support this hypothesis, and the same can be said about the increased (decreased) values of EGR (N). Furthermore, we do not find any significant temporal trends in cyclolysis or cyclogenesis (not shown) within the area of interest, which would indicate

that the number of cyclones remain fairly constant over time. To shed further light on the hypothesis of a local shift in the storm track, we correlated the DJF cyclone densities in Region B and C (where the most significant changes are found). Indeed there is a significant, negative correlation between these ($R = -0.54$, p -value = .005).

4 | DISCUSSION AND CONCLUSIONS

In this study, we have investigated changes in cyclone activity over the high-latitude North Atlantic and their regional consequences applying a storm-tracking algorithm on ERAI 1979–2016 MSLP fields along with a composite analysis. We found the strongest significant ($p < .1$) trends in cyclone density in DJF with positive trends around Svalbard (1.3 cyclone track points per decade in Region A and 3.0 cyclone track points per decade in Region B) and negative trends in the southeastern Barents Sea (-4.5 cyclone track points per decade, Region C). A similar hotspot of DJF cyclone density increase around Svalbard and in the Barents Sea was found by Zahn *et al.* (2018) and Rudeva and Simmonds (2015). The strength of the positive trend and the exact location of this hotspot, though, vary slightly between the studies.

These discrepancies likely result from differences in the time periods analysed, the tracking algorithms used, and the geographical binning applied. However, comparing our results to those of Zahn *et al.* (2018) and Rudeva and Simmonds (2015), we can probably exclude the role of the tracking algorithms in generating differences. The tracking algorithms used in these studies are shown to produce very similar results (schemes M10 and M22 in Fig. 1 in Neu *et al.* (2013)).

However, unlike previous studies (Dong *et al.*, 2013; Rudeva and Simmonds, 2015; Tamarin-Brodsky and Kaspi, 2017; Zahn *et al.*, 2018), we also addressed the regional consequences of cyclone activity in regions showing changes over the last decades. Our study is the first to extend the scope of a cyclone density change study to local consequences in the northernmost North Atlantic. Applying composite analysis, we found cyclone activity in Regions A and B to co-occur with positive surface temperature and precipitation anomalies over Svalbard and larger parts of the Barents Sea. These manifest alongside a higher energy content of the atmospheric column, as seen by the convergence of the vertically integrated transport of dry static energy and latent heat, and a reduced net ocean surface heat loss via radiative and turbulent fluxes and a shallower Z500–Z1000 layer in the same region. The corresponding anomalies for cyclone activity in Region C are broadly similar in geographic extent, however, with opposite signs.

We found a significant negative correlation between winter cyclone densities in the northwestern (Region B) and southeastern (Region C) Barents Sea, and simultaneously no significant increase in cyclogenesis or cyclolysis in the high-latitude North Atlantic. Based on these findings, we hypothesize that a shift toward a more meridional DJF storm track in this region is responsible for the documented positive (negative) trend in cyclone density in Region B (Region C). A significant decrease in Brunt–Väisälä frequency in Region B and an increase in Eady Growth Rate north of Regions A and B support an increase in baroclinicity and, hence, enhanced cyclone activity in this region. Further, the significant correlations between SCA and cyclone densities have the best match geographically with the regions where there are significant changes in cyclone densities (Regions A, B and C). Also, SCA is the climate index with a positive (though not significant) trend over the study period, which is qualitatively in line with an increased frequency of a more meridional storm track.

Several studies have addressed the question of how climate change alters baroclinic zones and, hence, storm tracks activity (Dong *et al.*, 2013; and others). A poleward shift of the storm track is reported by a majority of these studies and, in addition, Tamarin-Brodsky and

Kaspi (2017) report an enhanced poleward propagation of cyclones with the climate change. Our results with significant increases in cyclone density in the north (Regions A and B) and significant decreases the south (Region C) agree well with these results on a regional scale.

The areas in the western Barents Sea and around Svalbard, where we find significant positive trends in cyclone densities in winter (Regions A and B), have also experienced other rapid recent changes. These include the globally highest rates of wintertime 2 m air temperature increase (Førland *et al.*, 2011; Kohnemann *et al.*, 2017) and the most rapid winter sea ice decline (Parkinson and Cavalieri, 2008; Screen and Simmonds, 2010). In addition, Årthun *et al.* (2012) show that the oceanic heat inflow into the Barents Sea has increased and that this inflow controls the location of the sea ice margin in the western Barents Sea. The absence of sea ice during winter strongly alters the surface heat exchange and stratification of the air column and, hence, potentially leads to changes in cyclone intensification and dissipation (e.g. Kuo *et al.*, 1991; Jaiser *et al.*, 2012). Jaiser *et al.* (2012) further showed how the reduced stratification modulates the complex interactions of baroclinic wave energy fluxes on time-scales of a few days. Koyama *et al.* (2017) examined the possible connection between the recent Arctic sea ice loss and pan-Arctic cyclone activity. They found changes in baroclinicity suggesting an increased potential for cyclogenesis in years with low sea ice extent. Possible reasons for this could be more moisture available, regional baroclinicity, and vertical stability changes, all favouring cyclogenesis. However, when tracking individual cyclones, Koyama *et al.* (2017) did not observe a coherent increase in either cyclone frequency or intensity associated with sea ice loss.

We found cyclone activity in Regions A and B to co-occur with positive surface temperature and precipitation anomalies over Svalbard and large parts of the Barents Sea. With the large relative increase in cyclone occurrence in Regions A and B (Figure 2) and the documented increases in extreme cyclones in the region (Koyama *et al.*, 2017), there is a risk of increasing harmful (even devastating) impacts of cyclones in the Svalbard region. Especially in times with rapidly diminishing sea ice extent and rising DJF air temperatures, the additional heat and momentum from an individual cyclone might be enough to start winter melt and break-up of sea ice. Examples of high-impact wintertime cyclone events include the December 2015 storm *Frank* bringing above-zero temperatures to the North Pole (Boisvert *et al.*, 2016; Kim *et al.*, 2017; Yamagami *et al.*, 2017; Hong *et al.*, 2019). Also worth mentioning are the rain-on-snow events, such as those documented by Hansen *et al.* (2019). High-precipitation events in autumn and winter have led to destructive avalanches (Hancock *et al.*, 2018) in Svalbard.

Regional changes in cyclones, such as the increase in wintertime cyclone density over the Fram Strait found in this study, may also impact local ocean circulation. For example, Nilsen *et al.* (2016) found that an enhanced dominance of southerly wind stress, induced by the aforementioned increased cyclone densities, resulted in an increased inflow of Atlantic water into the fjords of western Spitsbergen. In turn, Luckman *et al.* (2015) found such intrusions of warm water into the fjords to be an important control of calving rates of maritime-terminating glaciers on Svalbard.

Despite reporting significant trends in cyclone occurrence for the time period 1979–2016, our results do not allow prediction of future changes in cyclones in our study region. In general, current climate models do not predict considerable intensification (deepening) of extratropical cyclones (Li *et al.*, 2014). This is, however, possibly due to challenges in modelling the factors affecting cyclone activity, which is sensitive to model resolution, atmosphere–ocean coupling, and parametrization of subgrid-scale physical processes (Willison *et al.*, 2013). Also, projected shifts in the storm tracks are a sum of several competing factors, an example being changing temperature gradients at different altitudes (Harvey *et al.*, 2014).

Focusing on the northern North Atlantic, both the historical and future changes in cyclone activity are primarily controlled by the factors affecting baroclinicity. Due to the competing effects of (a) the amplified Arctic warming, reducing the meridional temperature gradient and hence decreasing *EGR*, and (b) sea ice decline, reducing stratification and hence increasing *EGR*, the observed changes have varied between regions and also the future changes will depend on the region and time-scale addressed. Recent papers have suggested that wintertime cyclone activity in the Arctic will decrease toward the end of the century (Tamarin-Brodsky and Kaspi, 2017; Day *et al.*, 2018). However, the two competing effects on *EGR* may make the changes hard to model reliably. Further, due to sea ice loss and reduced boundary-layer stratification, near-surface winds over the northern Barents Sea and Svalbard region are in any case projected to increase (Ruosteenoja *et al.*, 2019), which, together with higher air temperatures, are expected to increase the impacts of cyclones.

ACKNOWLEDGEMENTS

We acknowledge the Academy of Finland (contract 317999) for supporting Timo Vihma's contribution to this manuscript.

ORCID

S. Wickström  <https://orcid.org/0000-0003-3650-844X>

REFERENCES

- Aagaard, K. and Greisman, P. (1975) Toward new mass and heat budgets for the Arctic Ocean. *Journal of Geophysical Research*, 80(27), 3821–3827. <https://doi.org/10.1029/JC080i027p03821>.
- Árthun, M., Eldevik, T., Smedsrud, L.H., Skagseth, Ø. and Ingvaldsen, R.B. (2012) Quantifying the influence of Atlantic heat on Barents Sea ice variability and retreat. *Journal of Climate*, 25(13), 4736–4743. <https://doi.org/10.1175/jcli-d-11-00466.1>.
- Barnston, A.G. and Livezey, R.E. (1987) Classification, seasonality and persistence of low-frequency atmospheric circulation patterns. *Monthly Weather Review*, 115(6), 1083–1126. [https://doi.org/10.1175/1520-0493\(1987\)115<1083:csapol>2.0.co;2](https://doi.org/10.1175/1520-0493(1987)115<1083:csapol>2.0.co;2).
- Bengtsson, L., Hodges, K.I. and Roeckner, E. (2006) Storm tracks and climate change. *Journal of Climate*, 19(15), 3518–3543. <https://doi.org/10.1175/jcli3815.1>.
- Boisvert, L.N., Petty, A.A. and Stroeve, J.C. (2016) The impact of the extreme winter 2015/16 Arctic cyclone on the Barents–Kara Seas. *Monthly Weather Review*, 144(11), 4279–4287. <https://doi.org/10.1175/mwr-d-16-0234.1>.
- Bueh, C. and Nakamura, H. (2007) Scandinavian pattern and its climatic impact. *Quarterly Journal of the Royal Meteorological Society*, 133(629), 2117–2131. <https://doi.org/10.1002/qj.173>.
- Cohen, J., Screen, J.A., Furtado, J.C., Barlow, M., Whittleston, D., Coumou, D., Francis, J., Dethloff, K., Entekhabi, D., Overland, J. and Jones, J. (2014) Recent Arctic amplification and extreme mid-latitude weather. *Nature Geoscience*, 7(9), 627–637. <https://doi.org/10.1038/ngeo2234>.
- Cottier, F.R., Nilsen, F., Inall, M.E., Gerland, S., Tverberg, V. and Svendsen, H. (2007) Wintertime warming of an Arctic shelf in response to large-scale atmospheric circulation. *Geophysical Research Letters*, 34(10), 607–612. <https://doi.org/10.1029/2007GL029948>.
- Day, J.J., Holland, M.M. and Hodges, K.I. (2018) Seasonal differences in the response of Arctic cyclones to climate change in CESM1. *Climate Dynamics*, 50(9–10), 3885–3903. <https://doi.org/10.1007/s00382-017-3767-x>.
- Dee, D.P., Uppala, S.M., Simmons, A.J., Berrisford, P., Poli, P., Kobayashi, S., Andrae, U., Balmaseda, M.A., Balsamo, G., Bauer, P., Bechtold, P., Beljaars, A.C.M., van de Berg, L., Bidlot, J., Bormann, N., Delsol, C., Dragani, R., Fuentes, M., Geer, A.J., Haimberger, L., Healy, S.B., Hersbach, H., Hólm, E.V., Isaksen, I., Kållberg, P., Köhler, M., Matricardi, M., McNally, A.P., Monge-Sanz, B.M., Morcrette, J.J., Park, B.K., Peubey, C., de Rosnay, P., Tavolato, C., Thépaut, J.-N. and Vitart, F. (2011) The ERA-Interim reanalysis: configuration and performance of the data assimilation system. *Quarterly Journal of the Royal Meteorological Society*, 137(656), 553–597.
- Dong, B., Sutton, R.T., Woollings, T. and Hodges, K. (2013) Variability of the North Atlantic summer storm track: mechanisms and impacts on European climate. *Environmental Research Letters*, 8(3), 034037.
- Dufour, A., Zolina, O. and Gulev, S.K. (2016) Atmospheric moisture transport to the Arctic: assessment of reanalyses and analysis of transport components. *Journal of Climate*, 29(14), 5061–5081. <https://doi.org/10.1175/jcli-d-15-0559.1>.

- Eady, E.T. (1949) Long waves and cyclone waves. *Tellus*, 1(3), 33–52. <https://doi.org/10.1111/j.2153-3490.1949.tb01265.x>.
- Ebita, A., Kobayashi, S., Ota, Y., Moriya, M., Kumabe, R., Onogi, K., Harada, Y., Yasui, S., Miyaoka, K., Takahashi, K., Kamahori, H., Kobayashi, C., Endo, H., Soma, M., Oikawa, Y. and Ishimizu, T. (2011) The Japanese 55-year reanalysis “JRA-55”: an interim report. *Scientific Online Letters on the Atmosphere*, 7, 149–152. <https://doi.org/10.2151/sola.2011-038>.
- Førland, E.J., Benestad, R., Hanssen-Bauer, I., Haugen, J.E. and Skaugen, T.E. (2011) Temperature and precipitation development at Svalbard 1900–2100. *Advances in Meteorology*, 2011, 1–14. <https://doi.org/10.1155/2011/893790>.
- Gelaro, R., McCarty, W., Suárez, M.J., Todling, R., Molod, A., Takacs, L., Randles, C.A., Darmenov, A., Bosilovich, M.G., Reichle, R., Wargan, K., Coy, L., Cullather, R., Draper, C., Akella, S., Buchard, V., Conaty, A., da Silva, A.M., Gu, W., Kim, G.K., Koster, R., Lucchesi, R., Merkova, D., Nielsen, J.E., Partyka, G., Pawson, S., Putman, W., Rienecker, M., Schubert, S.D., Sienkiewicz, M. and Zhao, B. (2017) The Modern-Era Retrospective analysis for Research and Applications, version 2 (MERRA-2). *Journal of Climate*, 30(14), 5419–5454. <https://doi.org/10.1175/jcli-d-16-0758.1>.
- Hancock, H., Prokop, A., Eckerstorfer, M. and Hendriks, J. (2018) Combining high spatial resolution snow mapping and meteorological analyses to improve forecasting of destructive avalanches in Longyearbyen, Svalbard. *Cold Regions Science and Technology*, 154, 120–132.
- Hansen, B.B., Gamelon, M., Albon, S.D., Lee, A.M., Stien, A., Irvine, R.J., Sæther, B.E., Loe, L.E., Ropstad, E., Veiberg, V. and Grøtan, V. (2019) More frequent extreme climate events stabilize reindeer population dynamics. *Nature Communications*, 10(1), 1616.
- Harvey, B.J., Shaffrey, L.C. and Woollings, T.J. (2014) Equator-to-pole temperature differences and the extra-tropical storm track responses of the CMIP5 climate models. *Climate Dynamics*, 43(5–6), 1171–1182. <https://doi.org/10.1007/s00382-013-1883-9>.
- Hodges, K.I. (1995) Feature tracking on the unit sphere. *Monthly Weather Review*, 123(12), 3458–3465. [https://doi.org/10.1175/1520-0493\(1995\)123<3458:ftotus>2.0.co;2](https://doi.org/10.1175/1520-0493(1995)123<3458:ftotus>2.0.co;2).
- Hong, J.-Y., Kim, B.-M., Baek, E.-H., Kim, J.-H., Zhang, X. and Kim, S.-J. (2019) A critical role of extreme Atlantic windstorms in Arctic warming. *Asia-Pacific Journal of Atmospheric Sciences*, 1–12. <https://doi.org/10.1007/s13143-019-00123-y>.
- Intergovernmental Panel on Climate Change. (2013) Climate Change 2013: The Physical Science Basis. In: Stocker, T.F., Qin, D., Plattner, G.-K., Tignor, M., Allen, S.K., Boschung, J., Nauels, A., Xia, Y., Bex, V. and Midgley, P.M. (Eds.) *Contribution of Working Group I to the Fifth Assessment Report of the Intergovernmental Panel on Climate Change*. Cambridge, UK and New York, NY: Cambridge University Press, pp. 1535.
- Isaksen, K., Nordli, Ø., Førland, E.J., Lupikasza, E., Eastwood, S. and Niedźwiedz, T. (2016) Recent warming on Spitsbergen – influence of atmospheric circulation and sea ice cover. *Journal of Geophysical Research: Atmospheres*, 121(20), 11913–11931. <https://doi.org/10.1002/2016JD025606>.
- Jaiser, R., Dethloff, K., Handorf, D., Rinke, A. and Cohen, J. (2012) Impact of sea ice cover changes on the Northern Hemisphere atmospheric winter circulation. *Tellus A*, 64(1), 11595. <https://doi.org/10.3402/tellusa.v64i0.11595>.
- Kendall, M.G. (1975) *Rank Correlation Methods*, 4th edition. London: Charles Griffin.
- Kim, B.-M., Hong, J.Y., Jun, S.Y., Zhang, X., Kwon, H., Kim, S.J., Kim, J.H., Kim, S.W. and Kim, H.K. (2017) Major cause of unprecedented Arctic warming in January 2016: critical role of an Atlantic windstorm. *Scientific Reports*, 7, 40051.
- Kobayashi, S., Ota, Y., Harada, Y., Ebita, A., Moriya, M., Onoda, H., Onogi, K., Kamahori, H., Kobayashi, C., Endo, H., Miyaoka, K. and Takahashi, K. (2015) The JRA-55 reanalysis: general specifications and basic characteristics. *Journal of the Meteorological Society of Japan, Series II*, 93(1), 5–48. <https://doi.org/10.2151/jmsj.2015-001>.
- Kohnemann, S.H.E., Heinemann, G., Bromwich, D.H. and Gutjahr, O. (2017) Extreme warming in the Kara Sea and Barents Sea during the winter period 2000–16. *Journal of Climate*, 30(22), 8913–8927. <https://doi.org/10.1175/jcli-d-16-0693.1>.
- Koyama, T., Stroeve, J., Cassano, J. and Crawford, A. (2017) Sea ice loss and Arctic cyclone activity from 1979 to 2014. *Journal of Climate*, 30(12), 4735–4754. <https://doi.org/10.1175/jcli-d-16-0542.1>.
- Kuo, Y.-H., Shapiro, M.A. and Donall, E.G. (1991) The interaction between baroclinic and diabatic processes in a numerical simulation of a rapidly intensifying extratropical marine cyclone. *Monthly Weather Review*, 119(2), 368–384. [https://doi.org/10.1175/1520-0493\(1991\)119<0368:tibbad>2.0.co;2](https://doi.org/10.1175/1520-0493(1991)119<0368:tibbad>2.0.co;2).
- Li, M., Woollings, T., Hodges, K. and Masato, G. (2014) Extratropical cyclones in a warmer, moister climate: a recent Atlantic analogue. *Geophysical Research Letters*, 41(23), 8594–8601. <https://doi.org/10.1002/2014GL02186>.
- Lim, E.-P. and Simmonds, I. (2009) Effect of tropospheric temperature change on the zonal mean circulation and SH winter extratropical cyclones. *Climate Dynamics*, 33(1), 19–32. <https://doi.org/10.1007/s00382-008-0444-0>.
- Lind, S., Ingvaldsen, R.B. and Furevik, T. (2018) Arctic warming hotspot in the northern Barents Sea linked to declining sea-ice import. *Nature Climate Change*, 8(7), 634–639. <https://doi.org/10.1038/s41558-018-0205-y>.
- Luckman, A., Benn, D.I., Cottier, F., Bevan, S., Nilsen, F. and Inall, M. (2015) Calving rates at tidewater glaciers vary strongly with ocean temperature. *Nature Communications*, 6(1), 8566. <https://doi.org/10.1038/ncomms9566>.
- Mann, H.B. (1945) Nonparametric tests against trend. *Econometrica: Journal of the Econometric Society*, 13(3), 245–259.
- Muckenhuber, S., Nilsen, F., Korosov, A. and Sandven, S. (2016) Sea ice cover in Isfjorden and Hornsund, Svalbard (2000–2014) from remote sensing data. *The Cryosphere*, 10(1), 149–158. <https://doi.org/10.5194/tc-10-149-2016>.
- Murray, R.J. and Simmonds, I. (1991) A numerical scheme for tracking cyclone centers from digital data. Part I: Development and operation of the scheme. *Australian Meteorological Magazine*, 39, 155–166.
- Naakka, T., Nygård, T. and Vihma, T. (2018) Arctic humidity inversions: climatology and processes. *Journal of Climate*, 31, 3765–3787. <https://doi.org/10.1175/JCLI-D-17-0497.1>.
- Naakka, T., Nygård, T., Vihma, T., Sedlar, J. and Graversen, R. (2019) Atmospheric moisture transport between mid-latitudes and the Arctic: regional, seasonal and vertical distributions. *International Journal of Climatology*, 39(6), 2862–2879. <https://doi.org/10.1002/joc.5988>.
- Nakamura, H., Sampe, T. and Tanimoto, Y. (2013) Observed associations among storm tracks, jet streams and midlatitude oceanic

- fronts. *Earth's Climate, Geophysical Monographs*, 147, 329–345. <https://doi.org/10.1029/147gm18>.
- Neu, U., Akperov, M.G., Bellenbaum, N., Benestad, R., Blender, R., Caballero, R., Coccozza, A., Dacre, H.F., Feng, Y., Fraedrich, K., Grieger, J., Gulev, S., Hanley, J., Hewson, T., Inatsu, M., Keay, K., Kew, S.F., Kindem, I., Leckebusch, G.C., Liberato, M.L.R., Lionello, P., Mokhov, I.I., Pinto, J.G., Raible, C.C., Reale, M., Rudeva, I., Schuster, M., Simmonds, I., Sinclair, M., Sprenger, M., Tilinina, N.D., Trigo, I.F., Ulbrich, S., Ulbrich, U., Wang, X.L. and Wernli, H. (2013) IMILAST: a community effort to intercompare extratropical cyclone detection and tracking algorithms. *Bulletin of the American Meteorological Society*, 94, 529–547. <https://doi.org/10.1175/BAMS-D-11-00154.1>.
- Nilsen, F., Cottier, F., Skogseth, R. and Mattsson, S. (2008) Fjord–shelf exchanges controlled by ice and brine production: the interannual variation of Atlantic water in Isfjorden, Svalbard. *Continental Shelf Research*, 28(14), 1838–1853. <https://doi.org/10.1016/j.csr.2008.04.015>.
- Nilsen, F., Skogseth, R., Vaardal-Lunde, J. and Inall, M. (2016) A simple shelf circulation model: intrusion of Atlantic water on the West Spitsbergen Shelf. *Journal of Physical Oceanography*, 46(4), 1209–1230. <https://doi.org/10.1175/jpo-d-15-0058.1>.
- Onarheim, I.H. and Árthun, M. (2017) Toward an ice-free Barents Sea. *Geophysical Research Letters*, 44(16), 8387–8395. <https://doi.org/10.1002/2017GL074304>.
- Onarheim, I.H., Eldevik, T., Árthun, M., Ingvaldsen, R.B. and Smedsrud, L.H. (2015) Skillful prediction of Barents Sea ice cover. *Geophysical Research Letters*, 42(13), 5364–5371. <https://doi.org/10.1002/2015GL064359>.
- Parkinson, C.L. and Cavalieri, D.J. (2008) Arctic sea ice variability and trends, 1979–2006. *Journal of Geophysical Research*, 113(C7), 1–28. <https://doi.org/10.1029/2007JC004558>.
- Petterssen, S. (1957) Weather observations, analysis, and forecasting. *Meteorological Research Reviews, Meteorological Monographs*, 3, 114–151. https://doi.org/10.1007/978-1-940033-25-9_1.
- Rinke, A., Maturilli, M., Graham, R.M., Matthes, H., Handorf, D., Cohen, L., Hudson, S.R. and Moore, J.C. (2017) Extreme cyclone events in the Arctic: wintertime variability and trends. *Environmental Research Letters*, 12(9), 094006. <https://doi.org/10.1088/1748-9326/aa7def>.
- Rudeva, I. and Simmonds, I. (2015) Variability and trends of global atmospheric frontal activity and links with large-scale modes of variability. *Journal of Climate*, 28(8), 3311–3330. <https://doi.org/10.1175/jcli-d-14-00458.1>.
- Ruosteenoja, K., Vihma, T. and Venäläinen, A. (2019) Projected changes in European and North Atlantic seasonal wind climate derived from CMIP5 simulations. *Journal of Climate*, 32(19), 6467–6490.
- Saha, S., Nadiga, S., Thiaw, C., Wang, J., Wang, W., Zhang, Q., van den Dool, H.M., Pan, H.L., Moorthi, S., Behringer, D., Stokes, D., Peña, M., Lord, S., White, G., Ebisuzaki, W., Peng, P. and Xie, P. (2006) The NCEP climate forecast system. *Journal of Climate*, 19(15), 3483–3517. <https://doi.org/10.1175/jcli3812.1>.
- Screen, J.A., Bracegirdle, T.J. and Simmonds, I. (2018) Polar climate change as manifest in atmospheric circulation. *Current Climate Change Reports*, 4(4), 383–395.
- Screen, J.A. and Simmonds, I. (2010) The central role of diminishing sea ice in recent Arctic temperature amplification. *Nature*, 464(7293), 1334–1337.
- Sen, P.K. (1968) Estimates of the regression coefficient based on Kendall's tau. *Journal of the American Statistical Association*, 63(324), 1379–1389.
- Sepp, M. and Jaagus, J. (2011) Changes in the activity and tracks of Arctic cyclones. *Climatic Change*, 105(3–4), 577–595. <https://doi.org/10.1007/s10584-010-9893-7>.
- Serreze, M.C. (1995) Climatological aspects of cyclone development and decay in the Arctic. *Atmosphere–Ocean*, 33(1), 1–23. <https://doi.org/10.1080/07055900.1995.9649522>.
- Serreze, M.C. and Barrett, A.P. (2008) The summer cyclone maximum over the central Arctic Ocean. *Journal of Climate*, 21(5), 1048–1065. <https://doi.org/10.1175/2007jcli1810.1>.
- Serreze, M.C., Box, J.E., Barry, R.G. and Walsh, J.E. (1993) Characteristics of Arctic synoptic activity, 1952–1989. *Meteorology and Atmospheric Physics*, 51(3–4), 147–164. <https://doi.org/10.1007/bf01030491>.
- Shepherd, T.G. (2014) Atmospheric circulation as a source of uncertainty in climate change projections. *Nature Geoscience*, 7(10), 703–708. <https://doi.org/10.1038/ngeo2253>.
- Simmonds, I., Burke, C. and Keay, K. (2008) Arctic climate change as manifest in cyclone behavior. *Journal of Climate*, 21(22), 5777–5796. <https://doi.org/10.1175/2008jcli2366.1>.
- Simmonds, I. and Lim, E.-P. (2009) Biases in the calculation of Southern Hemisphere mean baroclinic eddy growth rate. *Geophysical Research Letters*, 36(1), 115. <https://doi.org/10.1029/2008GL036320>.
- Simmonds, I. and Rudeva, I. (2014) A comparison of tracking methods for extreme cyclones in the Arctic basin. *Tellus A*, 66(1), 25252.
- Smedsrud, L.H., Ingvaldsen, R.B., Nilsen, J.E.Ø. and Skagseth, Ø. (2010) Heat in the Barents Sea: transport, storage, and surface fluxes. *Ocean Science*, 6(1), 219–234. <https://doi.org/10.5194/os-6-219-2010>.
- Sorteberg, A. and Walsh, J.E. (2008) Seasonal cyclone variability at 70°N and its impact on moisture transport into the Arctic. *Tellus A*, 60(3), 570–586. <https://doi.org/10.3402/tellusa.v60i3.15372>.
- Tamarin-Brodsky, T. and Kaspi, Y. (2017) Enhanced poleward propagation of storms under climate change. *Nature Geoscience*, 10(12), 908–913. <https://doi.org/10.1038/s41561-017-0001-8>.
- Theil, H. (1949) *A Rank-invariant Method of Linear and Polynomial Regression Analysis, 1-2; Confidence Regions for the Parameters of Linear Regression Equations in Two, Three and More Variables: (proceedings Knaw, _5_3(1950), Nr 3/4, Indagationes Mathematicae, _1_2(1950), P 85-91, P 173-177)*.
- Tsukernik, M., Kindig, D.N. and Serreze, M.C. (2007) Characteristics of winter cyclone activity in the northern North Atlantic: insights from observations and regional modeling. *Journal of Geophysical Research*, 112(D3), 1–19. <https://doi.org/10.1029/2006JD007184>.
- Vihma, T., Graversen, R., Chen, L., Handorf, D., Skific, N., Francis, J.A., Tyrrell, N., Hall, R., Hanna, E., Uotila, P., Dethloff, K., Karpechko, A.Y., Björnsson, H. and Overland, J.E. (2019) Effects of the tropospheric large-scale circulation on European winter temperatures during the period of amplified Arctic warming. Accepted for publication in *International Journal of Climatology*, 1–21. <https://doi.org/10.1002/joc.6225>.
- Vihma, T. and Pirazzini, R. (2005) On the factors controlling the snow surface and 2-m air temperatures over the Arctic Sea ice in winter. *Boundary-Layer Meteorology*, 117(1), 73–90. <https://doi.org/10.1007/s10546-004-5938-7>.

- Vihma, T., Screen, J., Tjernström, M., Newton, B., Zhang, X., Popova, V., Deser, C., Holland, M. and Prowse, T. (2016) The atmospheric role in the Arctic water cycle: a review on processes, past and future changes, and their impacts. *Journal of Geophysical Research: Biogeosciences*, 121(3), 586–620. <https://doi.org/10.1002/2015JG003132>.
- Wallace, J.M. and Hobbs, P.V. (2006) Introduction and overview. In *Atmospheric Science*, 2nd Edition, 1–23. New York, NY: Academic Press. <https://doi.org/10.1016/b978-0-12-732951-2.50006-5>.
- Willison, J., Robinson, W.A. and Lackmann, G.M. (2013) The importance of resolving mesoscale latent heating in the North Atlantic storm track. *Journal of the Atmospheric Sciences*, 70(7), 2234–2250. <https://doi.org/10.1175/jas-d-12-0226.1>.
- Yamagami, A., Matsueda, M. and Tanaka, H.L. (2017) Extreme Arctic cyclone in August 2016. *Atmospheric Science Letters*, 18(7), 307–314. <https://doi.org/10.1002/asl.757>.
- Yilmaz, A.G. and Perera, B.J.C. (2015) Spatiotemporal trend analysis of extreme rainfall events in Victoria, Australia. *Water Resources Management*, 29, 4465–4480.
- Zahn, M., Akperov, M., Rinke, A., Feser, F. and Mokhov, I.I. (2018) Trends of cyclone characteristics in the Arctic and their patterns from different reanalysis data. *Journal of Geophysical Research: Atmospheres*, 123(5), 2737–2751. <https://doi.org/10.1002/2017JD027439>.
- Zhang, X., Walsh, J., Zhang, J., Bhatt, U.S. and Ikeda, M. (2004) Climatology and interannual variability of Arctic cyclone activity: 1948–2002. *Journal of Climate*, 17(12), 2300–2317. [https://doi.org/10.1175/1520-0442\(2004\)017<2300:caivoa>2.0.co;2](https://doi.org/10.1175/1520-0442(2004)017<2300:caivoa>2.0.co;2).

How to cite this article: Wickström S, Jonassen MO, Vihma T, Uotila P. Trends in cyclones in the high-latitude North Atlantic during 1979–2016. *Q J R Meteorol Soc.* 2019;1–18. <https://doi.org/10.1002/qj.3707>



Graphic design: Communication Division, UIB / Print: Skjipes Kommunikasjon AS



uib.no

ISBN: 9788230855416 (print)
9788230862506 (PDF)